https://doi.org/10.1016/j.trc.2021.103146

Electric Vehicle Fleet Size for Carsharing Services Considering On-demand Charging Strategy and Battery Degradation

Min Xu[a], *Ting Wu*[a], *Zhijia Tan*[b]*

[a] *Department of Industrial and Systems Engineering, The Hong Kong Polytechnic University, Hung Hom, Hong Kong*

[b] *School of Maritime Economics and Management, Dalian Maritime University, Linghai Road 1, 116026 Dalian, PR China*

Abstract

This study addresses the tactical electric vehicle fleet size (EVFS) problem faced by carsharing service (CSS) providers while considering the operational vehicle assignment, vehicle relocation, and vehicle charging strategies (i.e., the charging duration at each station) in pursuit of profit maximization. To alleviate battery degradation and achieve cost-saving in the long term, we propose the on-demand charging strategy to determine fleet size. The novelty of this study lies in the incorporation of nonlinear battery wear cost incurred during the battery charging and discharging processes. A mixed-integer nonlinear programming (MINLP) model with concave and convex terms in the objective function is first developed for the EVFS problem. Piecewise linear approximation approach and outer-approximation method are employed to linearize the proposed model. Numerical experiments based on EVCARD, a one-way electric carsharing operator in China, are conducted to demonstrate the efficiency of the proposed model and solution method, as well as the necessity of incorporating the battery degradation into the fleet

* Corresponding author

Tel: +86-13871203424

Fax: ++86-0411-84726698

E-mail: zjatan@dlmu.edu.cn

size determination of CSSs. The impacts of several key parameters, i.e., the daily fixed cost of EV and battery price, battery cycle efficiency, service charge, and relocation cost on the performance of one-way electric CSSs are also analyzed.

Keywords: electric vehicle fleet size, on-demand charging strategy, battery wear cost, model linearization.

1. Introduction

As a new means of mobility service between public and private transport, CSS allows individuals to enjoy the convenience of private cars without owning them (Dill et al., 2019). It can be classified into round-trip and one-way services based on different vehicle return policies (Boyacı et al., 2015; Jorge et al., 2012; Jorge et al., 2014; Repoux et al., 2019). In the traditional round-trip CSSs, each vehicle has a designated parking spot and users are required to return vehicles to their pick-up locations. In contrast, in the one-way CSSs, users can drop off these vehicles at different stations. The flexibility of returning vehicles in one-way CSSs is attractive to users. Therefore, many carsharing operators provide one-way CSSs to users, e.g., EVCARD (EVCARD, 2020), GoFun (GoFun, 2020), Car2Go (Car2Go, 2020), and Smove (Smove, 2020). One-way CSSs can be further divided into free-floating and station-based (non-free-floating) systems according to the parking-spot restrictions (Boyacı and Zografos, 2019; Boyacı et al., 2015, 2017; Xu et al., 2018). The former allows users to pick up or drop off rented vehicles at any location of choice in an area with predetermined boundary, i.e., non-designated stations, whereas the latter imposes restrictions such that users can only pick up or drop off the cars at designated stations (Nourinejad et al., 2015; Xu et al., 2018). Convenient as they are, the one-way CSSs, however, would inevitably induce the vehicle imbalance problem across spatially distributed stations, i.e., the mismatch between the number of available vehicles at a specific station or an area and the user demand over a particular period (Lu et al., 2020; Wang et al., 2020; Yang et al., 2021). To alleviate the vehicle imbalance problem and thereby improve the performance of one-way CSSs, dynamic vehicle relocation operations between stations are imperative for the carsharing operators (Boyacı et al., 2015; Wang et al., 2019; Xu and Meng, 2019).

Over the past few years, electric vehicles (EVs) have gained increasing attention as a means of green transportation (Montoya et al., 2016; Schiffer and Walther, 2017).

A number of schemes have been promoted by governments to encourage the adoption of EVs, e.g., tax credits for the use of EVs in California, the access to bus and taxi lanes for EVs in Norway, and rebates towards the installation of public charging stations in New Hampshire (Cass and Grudnoff, 2017). Driven by these incentives, some carsharing operators have used EVs in their CSSs, e.g., EVCARD (EVCARD, 2020), AutoBleue (AutoBleue, 2020), and BlueSG (BlueSG, 2020). Although the adoption of EVs in CSSs is favorable as a demonstrably sustainable mobility solution, the limited driving range and frequent charging needs of EVs create inconvenience in operation and thus call for additional efforts in modeling and decision-making of CSSs. Moreover, EV batteries will suffer from severe degradation, e.g., a loss of battery capacity and a decrease of EV's driving range, caused by unhealthy charging and discharging processes (Barré et al., 2013; Pelletier et al., 2017). According to Pelletier et al. (2017), an EV battery is typically considered to have reached the end of its life when its available capacity decreases by 20% of its original value. Since the battery cost generally accounts for up to 35% of the total cost of an EV, battery degradation will lead to high battery wear cost and ultimately a reduction of overall profitability of CSSs, if not taken seriously. Therefore, special attention should be given to the characteristics of EVs, namely, the limited driving range, the charging requirement, and battery wear cost, in the decision-making of CSSs with EVs.

We focus in this study on station-based one-way electric CSSs. We aim to address a tactical EV fleet size problem by maximizing the profit of a carsharing operator while taking the dynamic vehicle relocation and battery degradation into consideration.

1.1. Literature review

The earliest studies for one-way CSSs focused on the decision-making problems of the gasoline vehicle fleet, including the determination of station location and capacity, fleet size, trip price, and vehicle relocation, etc. Readers may refer to the review articles

by Laporte et al. (2018) and Mourad et al. (2019) for more details. The recent introduction of EVs increases the managerial complexity as well as modeling and decision-making difficulty in CSSs due to their limited driving range per battery charge and their needs for charging infrastructure (Huang et al., 2020; Mounce et al., 2019). For the simplicity of modeling, the early attempts to consider an EV fleet in CSSs often make restrictive assumptions of vehicle charging, i.e., EV should stay at a station for a pre-specified time or should be charged to a certain level before it can be picked up by another user or relocator. This is referred to as 'strict' charging strategy thereafter. For example, Boyacı et al. (2015) built a multi-objective MILP model to deal with the strategic and tactical decisions for one-way CSSs by taking the vehicle relocation into account. Xu et al. (2018) investigated an EV fleet size and trip pricing problem considering vehicle relocation and personnel assignment by developing a mixed-integer convex programming model. Li et al. (2016) addressed the design of an EV sharing system considering both longer-term station location as well as fleet size planning and daily vehicle operations using a Continuum Approximation model. Both Boyacı et al. (2015), Xu et al. (2018), and Li et al. (2016) assumed that an EV had to be charged fully or for a fixed period of time in a station after each rental operation or relocation task. Unfortunately, 'strict' charging strategy would discourage the utilization of vehicles at peak-demand period because vehicles are forced to be charged even though the incumbent state of charge (SOC) is able to cover the electricity consumption of next trip. To circumvent this limitation, a few studies have relaxed the aforementioned assumption by allowing 'partial' charging (Boyacı and Zografos, 2019; Boyacı et al., 2017; Bruglieri et al., 2014; Bruglieri et al., 2017, 2019; Gambella et al., 2018; Hua et al., 2019; Xu and Meng, 2019; Zhang et al., 2019; Zhao et al., 2018), i.e., an EV can be picked up by a user or a relocator as long as its SOC is feasible for the next trip. As expected, the 'partial' charging strategy can cope with the demand surge at peak-demand period and improve the overall system performance. Table 1 indicates the

charging strategy considered in each of these studies for CSSs of EVs.

Table 1. Particulars of previous studies on the one-way electric CSSs

Authors	Charging strategy			Battery health consideration
	SC	PC	OC	
Gambella et al. (2018)	×	√	×	×
Bruglieri et al. (2014)	×	√	×	×
Xu and Meng (2019)	×	√	×	×
Boyacı et al. (2015)	√	×	×	×
Li et al. (2016)	√	×	×	×
Xu et al. (2018)	√	×	×	×
Zhang et al. (2019)	×	√	×	×
Boyacı and Zografos (2019)	×	√	×	×
Boyacı et al. (2017)	×	√	×	×
Bruglieri et al. (2017)	×	√	×	×
Bruglieri et al. (2019)	×	√	×	×
Zhao et al. (2018)	×	√	×	×
Hua et al. (2019)	×	√	×	×

Charging strategy: SC: Strict charging; **PC:** Partial charging; **OC:** On-demand charging

Although many studies have considered the limited driving range and charging requirement of EVs, none of them consider the battery health and impact of battery degradation. In fact, these studies implicitly assumed that EVs will always remain charged as long as they are idle at stations, disregarding how much electricity is actually needed for the next trip. This assumption may result in 'battery over-charged than needed', especially at the low-demand period, and unfavorably incur battery wear cost caused by battery degradation. Let us illustrate this issue using a simple example with one rental and one EV. Suppose we have an EV with 40% SOC and this EV needs to serve a rental with electricity consumption of 50%. The time allowed for charging is sufficient. To satisfy the rental, two charging schemes are proposed. The first charging scheme requires the EV to be fully charged before being assigned to the rental, whereas in the second charging scheme, this EV will be charged to 50% only and remain uncharged in the station until being picked up. It can be seen that both charging schemes make sure that the SOC of EV is feasible to serve the rental. Figure 1 shows the profiles

of SOC under the two schemes. According to Pelletier et al. (2017) and Han et al. (2014), the health of batteries is adversely affected by battery degradation occurring during charging and discharging processes corresponding to cycle aging, and the degradation of a battery will be more serious at high SOC, i.e., operating an EV at a higher value of SOC will lead to a higher battery wear cost. It should be noted that overcharging and over-discharging degradations are not considered in this study due to the function of overcharging and over-discharging protection in batteries. Therefore, the second charging scheme is better. This example demonstrates the necessity of designing an 'on-demand' charging strategy that not only allows flexible 'partial' charging but also charges EVs as per the need (instead of charging extensively as long as time allows), where the main concern is to reduce the battery degradation and wear cost for the sake of battery health as well as the profitability of CSSs in a long term.

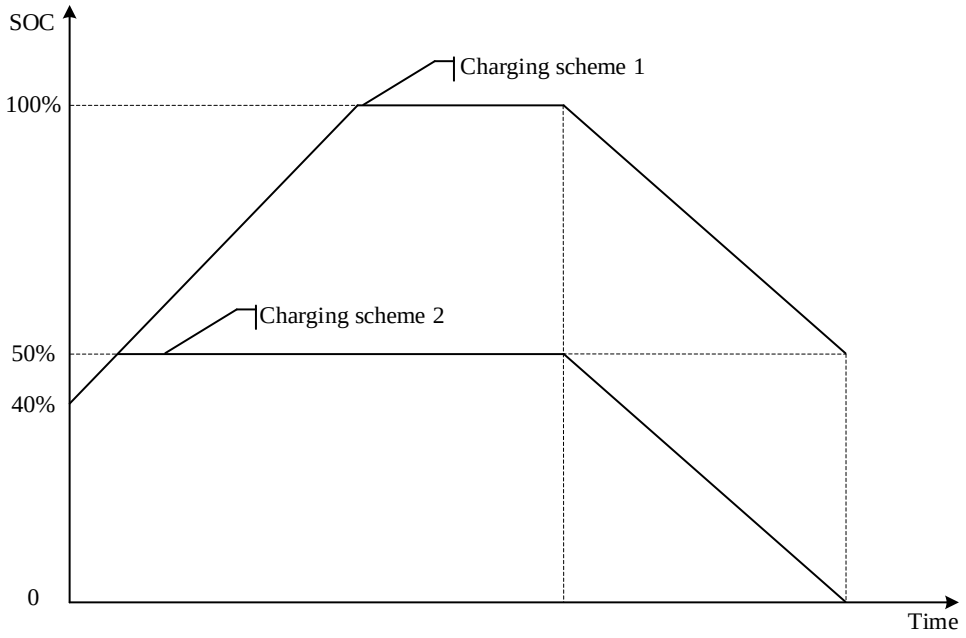

Figure 1. The SOC profiles of the EV under two charging schemes

Important as it is, to the best of our knowledge, no studies have ever considered the battery health or the 'on-demand' charging strategy in the electric CSSs (see Table

1). In this study, we will close this research gap by incorporating battery degradation from a cost perspective in the determination of EV fleet size for CSSs. We consider the nonlinear battery wear cost incurred during both the battery charging and discharging processes. The objective of this study is to determine the optimal tactical EV fleet size while considering the operational trip assignment, vehicle relocation, and 'on-demand' vehicle charging strategy that maximizes the daily profit of a carsharing operator. To achieve the objective, we will formulate a mixed-integer programming model by explicitly incorporating the nonlinear battery wear cost function (BWCF). The nonlinearity of BWCF makes the model unable to be efficiently solved by state-of-the-art solvers. We thus employ the outer-approximation approach and piecewise linear approximation technique to obtain the ε-optimal solution to the problem. Here the ε-optimal solution refers to the solution that the error of its objective function value to the optimal objective function value is within an exogenously pre-specified maximum tolerance ε.

The remainder of this study is organized as follows. Assumptions and problem statement are presented in Section 2. An MINLP model for the EVFS problem is formulated in Section 3. Section 4 discusses the model properties and linearizes the BWCF by employing the outer-approximation method and piecewise linear approximation approach. The resultant MILP model can be readily solved by available solvers to obtain the ε-optimal solution. The efficiency of the proposed model and solution method, as well as the necessity of incorporating the battery degradation into the fleet size determination of CSSs are demonstrated in Subsection 5.2 and Subsection 5.3, respectively, through numerical experiments based on EVCARD in China. Section 6 presents the conclusions and discusses future research directions.

2. Assumptions and Problem Description

Consider a one-way CSS provider who operates a fleet of homogenous EVs among

a number of predetermined stations in an urban area. At the beginning of the service operation, the EVs are initially distributed at different stations. During the operation period, users are allowed to pick up vehicles according to their reservations and return them later at another station different from their pick-up stations. The information of all rentals, i.e., CSS orders, requested from users is assumed to be known a priori by estimation/prediction or reservation. In order to achieve profit maximization, not all demands are to be satisfied due to the limited resources, and a penalty will be incurred if a customer is denied service. The distribution of EVs across stations will become imbalanced along with the flow dynamics of users. EVs will be relocated among these stations to address vehicle imbalance and demand asymmetry problems. Considering the limited driving range of EVs, it is assumed that sufficient parking spots equipped with charging facilities are provided in each station such that EVs can be charged when staying idle at stations. The battery will be discharged when relocated or under service. For simplicity, we assume that the SOC of EVs will increase/decrease linearly with charging/discharging time, with battery wear cost incurred according to a battery wear cost model to be introduced in Subsection 2.1. The EVFS problem aims to maximize the daily profit of CSS providers by determining the EV fleet size considering the vehicle assignment, vehicle relocation, and 'on-demand' vehicle charging strategy.

2.1. Battery wear cost

Battery degradation occurs during charging and discharging processes corresponding to cycle aging. Based on the experimental cycle life data of EVs provided by the manufacturers, Han et al. (2014) proposed the following generic semi-empirical battery wear cost model for EVs:

$$WC = BS \times \int_{l_{init}}^{l_{ulti}} W(l)\left|dl\right| \tag{1}$$

where WC denotes the battery wear cost incurred during charging or discharging

process when the SOC increases or decreases from l_{init} to l_{ulti}; BS represents the battery size measured in kWh; $W(l)$ is the battery wear density function that represents the battery wear cost per unit energy transfer at the SOC l, given by

$$W(l) = \frac{BP \times b}{2 \times BS \times \mu^2 \times a} \times (1-l)^{b-1} \tag{2}$$

where BP is the battery price of an EV; a and b are battery-dependent parameters that are acquired experimentally and we have $0 < b < 1$ and $a > 0$; μ is the battery cycle efficiency.

It's easy to see that the battery wear density function $W(l)$ is a monotonically increasing function with respect to the SOC l. The wear cost per unit energy transfer is thus higher when a battery is operated at a higher value of SOC. By further substituting Eq. (2) into Eq. (1), with simple manipulation, we can obtain the following explicit expression of battery wear function:

$$WC = \frac{BP}{2 \times \mu^2 \times a} \times \left| (1-l_{init})^b - (1-l_{ulti})^b \right| \tag{3}$$

We can see that the battery wear cost depends not only on the charging/discharging amount, i.e., charging/discharging duration, but also the initial SOC before charging/discharging.

The consideration of battery wear cost would significantly affect the optimal vehicle assignment for cost minimization or profit maximization. This can be illustrated by a simple example with three stations, i.e., Station A, Station B, and Station C, two rentals, i.e., Rental 1 and Rental 2, and two EVs, i.e., EV 1 and EV 2. Suppose Rental 1 departs from Station A to Station B with electricity consumption of 30% and Rental 2 departs from Station A to Station C with electricity consumption of 40%. Both the

two EVs are available at Station A, with initial SOCs 60% (EV 1) and 70% (EV 2), respectively. We first consider the greedy assignment strategy, i.e., Strategy 1, that assigns a rental with more electricity consumption to an EV with higher SOC. By this strategy, Rental 1 will be assigned to EV 1, while Rental 2 will be assigned to EV 2. The SOC profiles of the two EVs under Strategy 1 are illustrated in Figure 2 (a). On the other hand, if we choose another way by assigning Rental 1 to EV 2 and assigning Rental 2 to EV 1, referred to as Strategy 2, the variations of SOC will become the profiles shown in Figure 2 (b). We can see that Rental 1 and Rental 2 can be satisfied in both strategies. Since $W(l)$ is an increasing function with respect to l, the total battery wear cost of Strategy 2 is less than Strategy 1. Therefore, Strategy 2 is better than Strategy 1 from the perspective of cost-saving. Hence, with battery wear cost taking into consideration, the vehicle assignment for the cost minimization or profit maximization would be largely influenced.

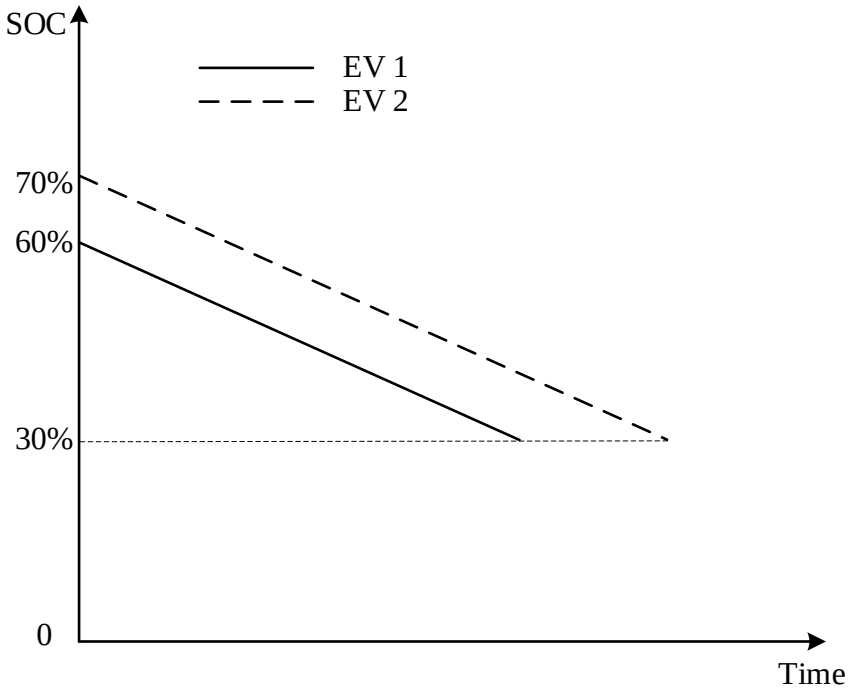

(a) The SOC profiles of the two EVs under Strategy 1

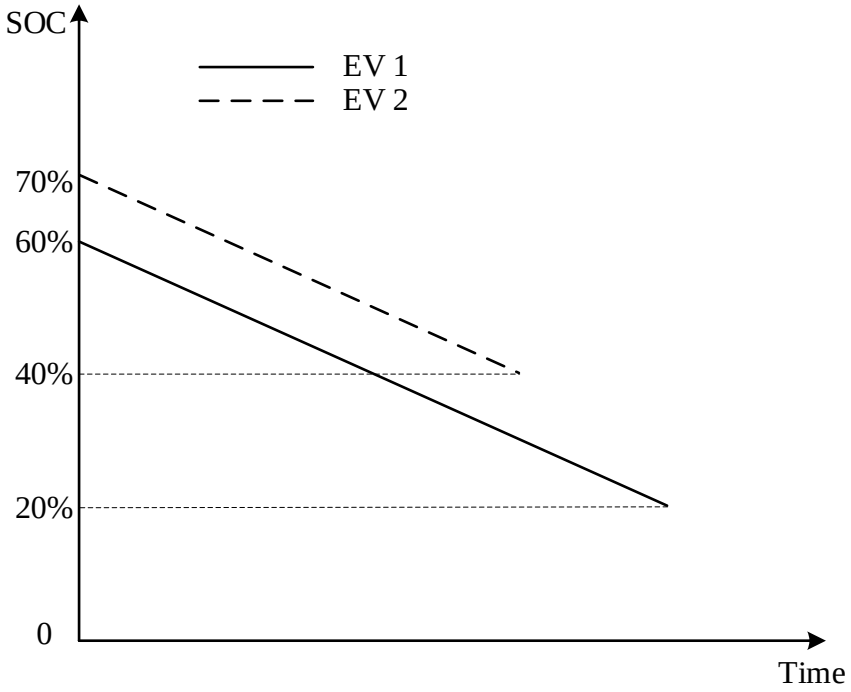

(b) The SOC profiles of the two EVs under Strategy 2

Figure 2. The SOC profiles of the two EVs under two vehicle assignment strategies

2.2. On-demand charging strategy

Apart from the vehicle assignment, the consideration of battery wear cost will also affect the schedule of vehicle relocation and vehicle charging. For example, suppose we have only one EV in the CSS with three stations, i.e., Station A, Station B, and Station C. The EV is available at Station A from 1:30 pm onwards, with initial SOC of 10%. There will be a rental departing from Station B to Station C at 3:00 pm and the travel time is 30 min. To serve this rental, a relocation operation from Station A to Station B is needed. We further assume that the relocation time from Station A to Station B is 30 min and the charging and discharging rates are 10% SOC variation per 15 min. Excluding the relocation time, there are 60 min available for charging, either at Station A or Station B. Considering the electricity consumption during vehicle relocation, the EV should be charged at Station A for at least 15 min in order to have enough electricity for relocation operation. We consider three feasible schedules of vehicle relocation and

vehicle charging in this example, i.e., Schedule 1, Schedule 2, and Schedule 3. Schedule 1 requires the EV to be charged at Station A for 60 min before the relocation operation to Station B, while under Schedule 2, after being charged for 15 min at Station A, the EV is relocated to Station B and charged at Station B for another 45 min. Unlike the aforementioned two schedules, under which the EV is charged as long as it stays idle at a station, Schedule 3 charges the EV as per the need, i.e., before and after the relocation operation, the EV is charged for 15 min and 30 min at Station A and Station B, respectively. Figure 3 shows the EV trajectories corresponding to the three schedules in a time-space coordinate system. The SOC profiles of EV under the three schedules are illustrated in Figure 4. We can see that the SOC of EV under Schedule 3 is averagely lower than the other two schedules, indicating that the battery wear cost under Schedule 3 is the least and thus, Schedule 3 is the best.

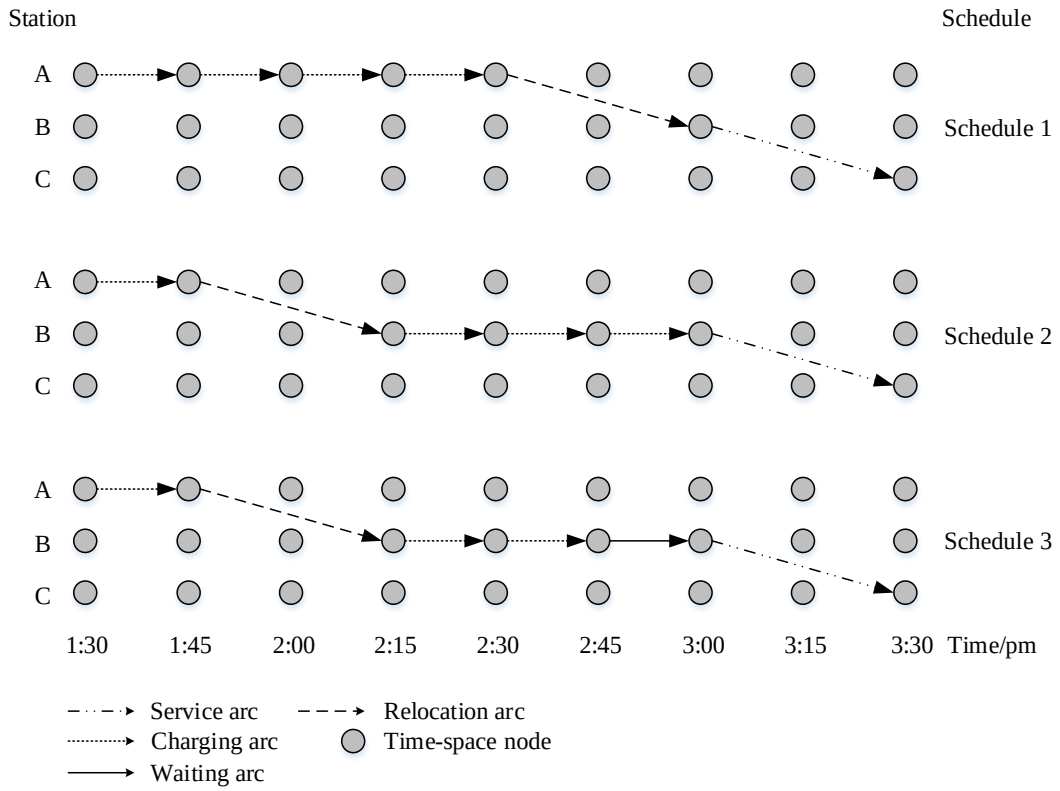

Figure 3. The EV trajectories under three schedules in a time-space coordinate system

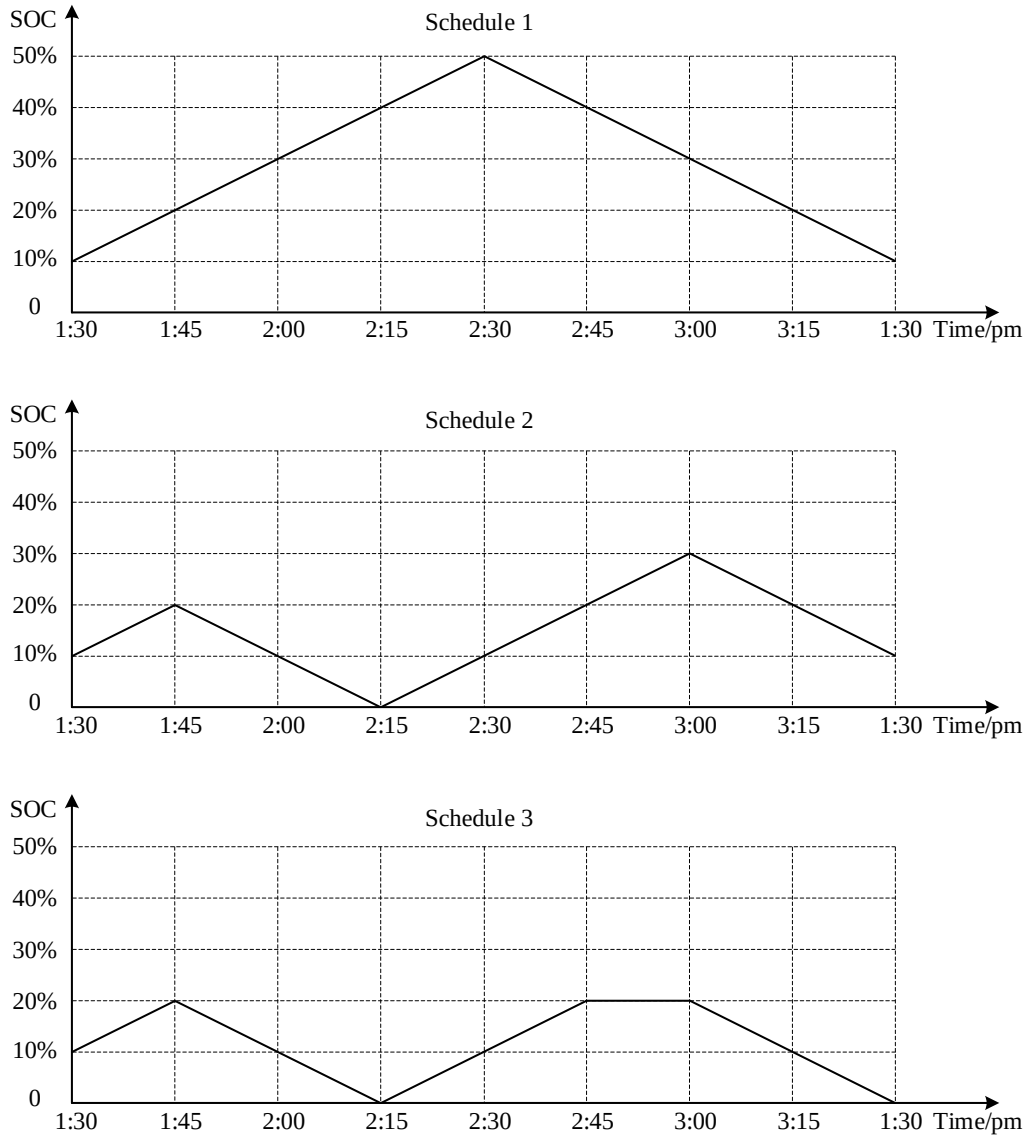

Figure 4. The SOC profiles of EV under three schedules

Instead of extensive charging whenever staying idle at stations, we consider 'on-demand' charging strategy that not only allows 'partial' charging of EVs before they are picked up but also charges the EVs as needed for the sake of battery health and cost-saving. The amount of electricity to be charged at each station should be determined jointly with the vehicle assignment and vehicle relocation.

3. Optimization Model Building

3.1. Notations

To formulate the EVFS problem, let FC be the fixed amortized cost of an EV per day and I denote the set of rentals. Each rental $i \in I$ is described by a quadruplet $U_i = \{s_i^o, s_i^d, t_i^o, t_i^d\}$, where s_i^o and s_i^d denote the pick-up and drop-off stations of rental $i \in I$, t_i^o and t_i^d denote the departure and arrival time of rental $i \in I$. Let l_i, TP_i and PC_i be the electricity consumption, net profit, and incurred penalty of rental $i \in I$, and l_{ij}, t_{ij} and RC_{ij} denote the electricity consumption, time, and cost of relocation operation from the drop-off station of rental i to the pick-up station of rental j, respectively. The electricity consumption and replenishment are measured by the variation of SOC of the battery. Because we assume linear charging and discharging process, both the charging and discharging rate, i.e., the uniform variation of SOC per unit of time, are represented by constants CR and DR, respectively. The usable battery capacity denoted by E is also measured by SOC, i.e., $E = 100\%$. Without loss of generality, we assume that $l_i \le E$, $\forall i \in I$. The minimum SOC value allowed for an EV is denoted by E_{min}.

For ease of model building, we create a dummy node denoted by n_0, which all vehicles will depart from and return to at the beginning and end of the operation period, respectively. In this way, the fleet size is exactly the number of EVs originating from the node n_0. It is assumed that the attributes of the dummy node (i.e., the electricity consumption, time duration, net profit, and incurred penalty) and the links (i.e., the electricity consumption, time, and cost) connecting the dummy node and the physical stations are zero. Let A^0 denote the set of dummy links connecting the dummy node

and all the rentals and A^r denote the set of relocation operations connecting any two rentals that are compatible both in terms of travel time and electricity consumption. In other words, a link (i, j), $\forall i \neq j \in I$ belongs to set A^r if it satisfies the following conditions:

$$t_{ij} \leq t_j^o - t_i^d \tag{4}$$

$$min\left\{E, E - l_i + CR \times (t_j^o - t_i^d - t_{ij})\right\} \geq l_{ij} \tag{5}$$

$$min\left\{E, E - l_i - l_{ij} + CR \times (t_j^o - t_i^d - t_{ij})\right\} \geq l_j \tag{6}$$

As for the decision variables, let f be an integer decision variable representing the fleet size of EVs, z_i be a binary decision variable that equals 1 if rental $i \in I$ is satisfied (and 0 otherwise), and x_{ij} be a binary decision variable that equals 1 if an EV is relocated from the drop-off station of rental i to the pick-up station of rental j (and 0 otherwise). On a typical operation day, an EV will depart from the dummy node. It then serves a series of rentals and gets charged at traversed stations before finally returning to the dummy node. The activity trajectory of an EV, which can be seen as a trip chain r consisting of a dummy node and a series of rentals sorted in ascending order in terms of their departure time, i.e., n_0, i_1, i_2, i_3,…, i_{m_r}, n_0, as well as several relocation operations connecting these rentals, can be intuitively represented by

$$n_0 \Rightarrow s_{i_1}^o \rightarrow s_{i_1}^d \Rightarrow s_{i_2}^o \rightarrow s_{i_2}^d \Rightarrow \cdots \Rightarrow s_{i_k}^o \rightarrow s_{i_k}^d \Rightarrow \cdots \Rightarrow s_{i_{m_r}}^o \rightarrow s_{i_{m_r}}^d \Rightarrow n_0 \tag{7}$$

where the single- and double-lined arrows denote the rentals and relocations from one station to another, respectively. To capture the SOC of EV and facilitate the formulation of 'on-demand' charging strategy, in addition to the aforementioned integer or binary variables, we define a set of continuous variables: two SOC-state variables, R_i and Q_i,

$\forall i \in I$, denoting the SOC of an EV rightly before serving the rental i and the relocation operation originated from the drop-off station of rental i, respectively; and two electricity-amount variables, e_i^o and e_i^d , $\forall i \in I$, denoting the amount of electricity charged at the pick-up station and drop-off station of rental $i \in I$, respectively. All the notations used throughout this study are provided in Appendix A for readability.

Suppose that the amount of electricity charged at the dummy node is zero. The EV departs from the dummy node with SOC expressed by $R_{i_1} - e_{i_1}$. After arriving at station $s_{i_1}^o$, it is charged to R_{i_1}. The same vehicle is then picked up by a user and the SOC reduces to $R_{i_1} - l_{i_1}$ when being dropped off at station $s_{i_1}^d$. By making use of the dwell time at station $s_{i_1}^d$, the EV is charged to Q_{i_1}. After being relocated to station $s_{i_2}^o$, the SOC falls to $Q_{i_1} - l_{i_1 i_2}$, which also equals $R_{i_2} - e_{i_2}$. Figure 5 illustrates the trajectory of the EV in a time-space coordinate system and Figure 6 shows the correspondent profile of SOC over the same period of time. The above process happens iteratively, and according to Eq. (1), there will be battery wear cost each time the SOC varies. By simple manipulation, we can obtain the following battery wear cost of an EV over the entire operation period:

$$WC_r = \frac{BP}{\mu^2 \times a} \times \sum_{k=1}^{m_r} [(1 - R_{i_k} + e_{i_k}^o)^b - (1 - R_{i_k})^b + (1 - R_{i_k} + l_{i_k})^b - (1 - Q_{i_k})^b] \quad (8)$$

Therefore, the total battery wear cost of all EVs is calculated by

$$TWC = C \sum_{i \in I} [(1 - R_i + e_i^o)^b - (1 - R_i)^b + (1 - R_i + l_i)^b - (1 - Q_i)^b] \quad (9)$$

where $C = \frac{BP}{\mu^2 \times a}$.

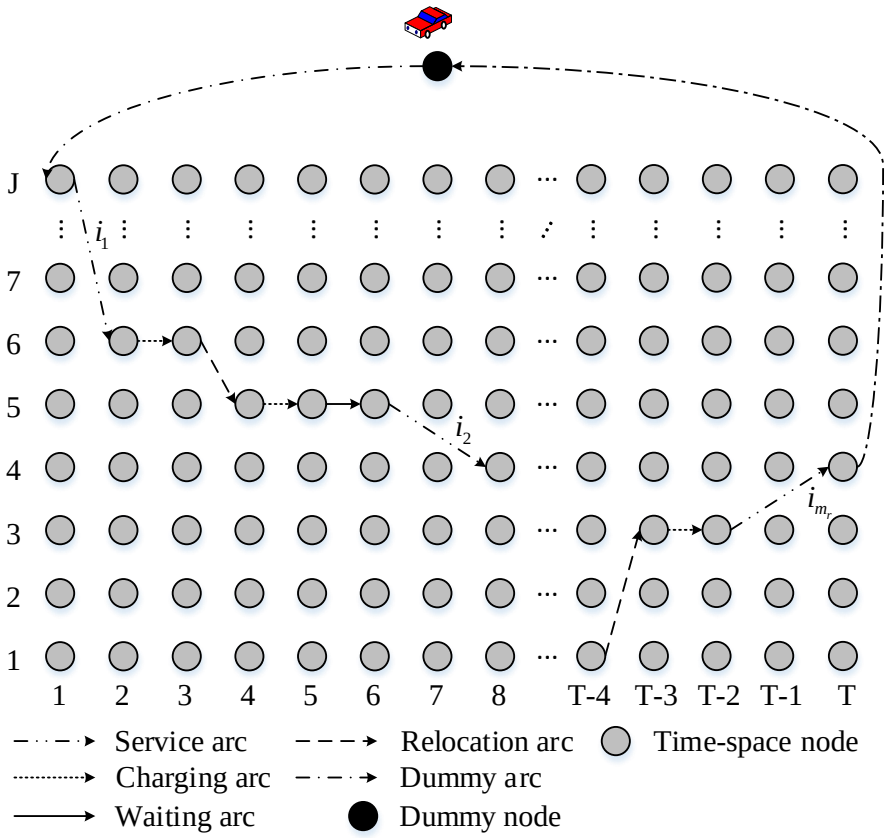

Figure 5. Trajectory of an EV in a time-space coordinate system over the operation period

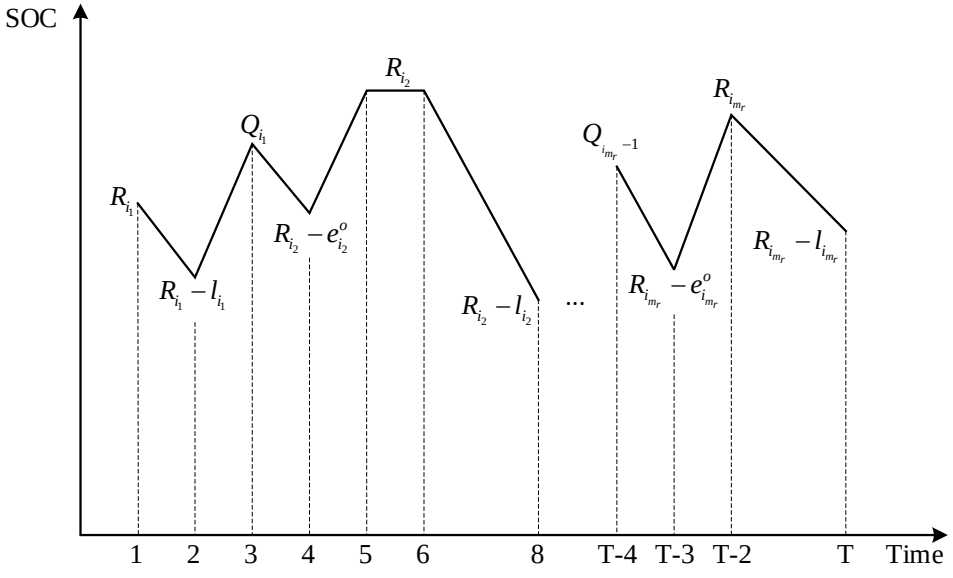

Figure 6. SOC profile of the EV in Figure 5

3.2. Model formulation

Given the above notations, the EVFS problem can be formulated as follows:

[EVFS]

$$\max_{\mathbf{x,z,f,R,Q,e}} PROFIT(\mathbf{x,z,f,R,Q,e}) = \sum_{i\in I} TP_i \times z_i - \sum_{i\in I} PC_i \times (1-z_i) - \sum_{(i,j)\in A^r} RC_{ij} \times x_{ij} - FC \times f - TWC \tag{10}$$

subject to Eq. (9) and

$$\sum_{i\in I\cup\{n_0\}:(i,j)\in A^0\cup A^r} x_{ij} = z_j, \quad \forall j \in I \tag{11}$$

$$\sum_{i\in I\cup\{n_0\}:(i,j)\in A^0\cup A^r} x_{ij} - \sum_{i\in I\cup\{n_0\}:(j,i)\in A^0\cup A^r} x_{ji} = 0, \quad \forall j \in I \tag{12}$$

$$\sum_{i\in I} x_{n_0 i} \le f \tag{13}$$

$$R_i \ge l_i + E_{min}\ z_i, \ \forall i \in I \tag{14}$$

$$Q_i \ge (l_{ij} + E_{min})x_{ij}, \quad \forall i \ne j \in I, (i,j) \in A^r \tag{15}$$

$$Q_i = R_i - l_i + e_i^d, \quad \forall i \in I \tag{16}$$

$$R_j \le Q_i - l_{ij} + e_j^o + M_1(1-x_{ij}), \quad \forall i \ne j \in I \cup \{n_0\}, (i,j) \in A^0 \cup A^r \tag{17}$$

$$t_i^d + \frac{e_i^d}{CR} + t_{ij}x_{ij} \le t_j^o - \frac{e_j^o}{CR} + M_2(1-x_{ij}), \quad \forall i \ne j \in I, (i,j) \in A^r \tag{18}$$

$$e_{n_0}^o = e_{n_0}^d := 0 \tag{19}$$

$$R_i, Q_i, e_i^o, e_i^d \in [0, E], \forall i \in I \cup \{n_0\} \tag{20}$$

$$f \in Z^+, x_{ij}, z_i \in \{0,1\}, \quad \forall (i,j) \in A^0 \cup A^r, i \in I \tag{21}$$

where $M_1 := E + max\{l_{ij}\}_{(i,j)\in A^r}$, $M_2 := max\{t_j^o\}_{j\in I} - min\{t_j^o\}_{j\in I} + E/CR$, and Z^+

denotes the set of non-negative integers.

The objective function shown by Eq. (10) is the daily profit of CSS providers, i.e., the difference of service revenue and total system cost. The cost is composed of four terms, including the penalty for unserved rentals, the relocation cost (e.g., the electricity consumption cost), the capital investment of the EV fleet, and the battery wear cost in sequence. Note that the battery wear cost in Eq. (10), i.e., TWC, is calculated by Eq. (9). Constraint (11) delineates the fulfillment of rentals, which ensures that there should be one EV arriving at the origin station of rental j if it is served, i.e., $z_j = 1$. Constraint (12) is the flow conservation constraint. Constraint (13) limits that the total number of EVs originating from the dummy node is not larger than the fleet size. Constraints (14)-(20) are constraints dedicated to the characteristics of EVs. Specifically, Constraints (14) and (15) ensure the feasibility of nodes (i.e., serving rentals) and links (i.e., relocation operations) in terms of the SOC of EV. Constraints (16) and (17) update the SOC upon the departure of EV to serve rentals and the relocation of EV to another station considering the charging and discharging processes, respectively. In particular, based on the recursion relationship, Constraint (17) updates the SOC-state variables of two rentals connected by a relocation operation. Note that since $M_1 = E + max\left\{l_{ij}\right\}_{(i,j)\in A^r}$, R_j will be $Q_i - l_{ij} + e_j^o$ at optimal if $x_{ij} = 1$. Constraint (18) ensures that the EVs are timely relocated in order to serve the next rental. Again this constraint reduces to $t_i^d + \frac{e_i^d}{CR} + t_{ij} \le t_j^o - \frac{e_j^o}{CR}$ at optimal if $x_{ij} = 1$ because $M_2 = max\left\{t_j^o\right\}_{j\in I} - min\left\{t_j^o\right\}_{j\in I} + E/CR$. Constraint (19) imposes that the amount of electricity charged at the dummy node is zero. Constraints (20) and (21) define the domains of variables x_{ij}, z_i, f, R_i, Q_i, e_i^o and e_i^d.

It is worth noting that the model [EVFS] can be easily extended to consider the

users' range anxiety, which, if not taken into account properly, may lower the level of CSSs significantly. The range anxiety here refers to the fear of running out of electricity before reaching the destinations (Xu et al., 2020). To achieve this, an additional constraint can be added and expressed by

$$R_i \geq l_i + E_{comf} \times z_i, \qquad \forall i \in I \tag{22}$$

where E_{comf} denotes the minimum SOC value above which users are free from range anxiety.

4. Model Properties and Model Linearization

It can be seen that except for the total battery wear cost term in Eq. (10), all the constraints and the other terms in the objective function are linear. The consideration of battery health results in a nonlinear model that is not easily solvable by commercial solvers. To address this problem, we first define another continuous variable, i.e., $G_i := R_i - e_i^o$, $\forall i \in I$, denoting the SOC of an EV rightly after arriving at the origin station of rental i. Then the battery wear cost term in the objective function (10) will become

$$MTWC = C\sum_{i \in I}[-(1-G_i)^b + (1-R_i)^b - (1-R_i+l_i)^b + (1-Q_i)^b] \tag{23}$$

It should be noted that $MTWC$ denotes the minus of total battery wear cost, i.e., $MTWC = -TWC$, by further taking the minus sign in the objective function (10) into consideration. For the convenience of description, the minus of total battery wear cost will be referred to as MTWC for short. By digging further, we can find that the MTWC in the above equation can be divided into three terms, i.e., $-(1-G_i)^b$, $(1-R_i)^b - (1-R_i+l_i)^b$ and $(1-Q_i)^b$. In other words, we can rewrite Eq. (23) as follows:

$$MTWC = C\left(\sum_{i\in I}\left(-(1-G_i)^b\right) + \sum_{i\in I}\left((1-R_i)^b - (1-R_i+l_i)^b\right) + \sum_{i\in I}(1-Q_i)^b \right) \quad (24)$$

Since $0<b<1$, it is not hard to prove that the term $-(1-G_i)^b$ is convex with respect to G_i, whereas $(1-R_i)^b-(1-R_i+l_i)^b$ and $(1-Q_i)^b$ are concave with respect to R_i and Q_i, respectively. Therefore, the model [EVFS] is an MINLP model with both concave and convex terms in the objective function subject to many linear constraints. To linearize the model, we will employ the piecewise linear approximation approach and outer-approximation method for the convex and concave terms, respectively. Details can be found in the next subsections.

4.1. Piecewise linear approximation approach

This subsection describes the linearization of the convex term of the MTWC, i.e., $-(1-G_i)^b$ in Eq. (24), in the objective function of the model [EVFS]. The piecewise linear approximation approach is one of the most prevailing linearization techniques for nonlinear separable programming problems. It works by approximating any arbitrary continuous function using a piecewise linear function, as illustrated in Figure 7. The error resulted from the approximation can be controlled by the number of linear segments. To apply the piecewise linear approximation approach for the model [EVFS], let $g(G_i)$ denote the convex term $-(1-G_i)^b$, i.e., $g(G_i) := -(1-G_i)^b$, $\forall G_i \in [0,E]$, $\forall i \in I$. As shown in Figure 7, the interval $[0,E]$ is subdivided into smaller intervals by the point $G_i^{(k)}$, where $k \in K = \{1,2,...,N-1,N\}$ and $0 = G_i^{(1)} < G_i^{(2)} < ... < G_i^{(N-1)} < G_i^{(N)} = E$. K is the set of breakpoints for the linear segments of the curve $g(G_i)$. Appendix B will present the generation of breakpoints for the linear segments such that the approximation of the function $g(G_i)$ can be

controlled within a pre-specified tolerance $\hat{\varepsilon}$. Any point G_i in the interval $[G_i^{(k)}, G_i^{(k+1)}]$ can be thus uniquely expressed as $G_i = \lambda_i^k G_i^{(k)} + \lambda_i^{k+1} G_i^{(k+1)}$, where $\lambda_i^k + \lambda_i^{k+1} = 1$, λ_i^k, $\lambda_i^{k+1} \geq 0$. Then $\hat{g}(G_i) = \lambda_i^k g(G_i^{(k)}) + \lambda_i^{k+1} g(G_i^{(k+1)})$ gives a linear approximation of the function $g(G_i)$ in the interval $[G_i^{(k)}, G_i^{(k+1)}]$. The piecewise linear approximation of the function $g(G_i)$ over the interval $[0, E]$ can then be written as $\hat{g}(G_i) = \sum_{k=1}^{N} \lambda_i^k g(G_i^{(k)})$, where $G_i = \sum_{k=1}^{N} \lambda_i^k G_i^{(k)}$, $\sum_{k=1}^{N} \lambda_i^k = 1$, and at most two adjacent λ_i^k are positive (often referred to as 'special ordered sets of type 2' (SOS2) in the literature (Guéret et al., 2000).

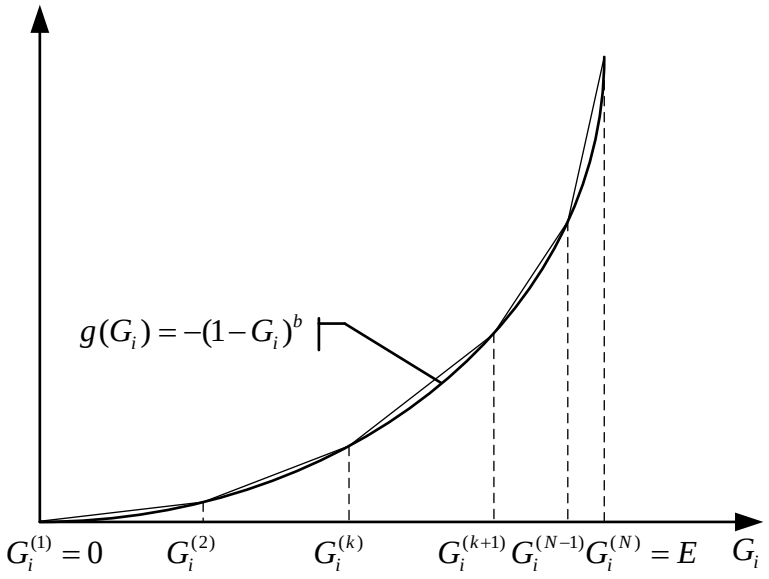

Figure 7. Illustration of piecewise linear approximation approach

A reformulated model [EVFS-I] can be obtained by replacing the convex term $-(1-G_i)^b$ in the objective function of model [EVFS] with the piecewise linear approximation $\hat{g}(G_i)$ and enforcing the associated conditions, i.e., Constraints (11)-

(21), and

$$\sum_{k=1}^{N} \lambda_i^k G_i^{(k)} = R_i - e_i^o \quad \forall i \in I \tag{25}$$

$$\sum_{k=1}^{N} \lambda_i^k = 1 \quad \forall i \in I \tag{26}$$

$$\sum_{k=1}^{N-1} \delta_i^k = 1 \quad \forall i \in I \tag{27}$$

$$\lambda_i^1 \le \delta_i^1 \quad \forall i \in I \tag{28}$$

$$\lambda_i^k \le \delta_i^{k-1} + \delta_i^k \quad \forall i \in I, k \in K \setminus \{1, N\} \tag{29}$$

$$\lambda_i^N \le \delta_i^{N-1} \quad \forall i \in I \tag{30}$$

$$\lambda_i^k \ge 0, \delta_i^k \in \{0,1\}, \quad \forall i \in I, k \in K \tag{31}$$

where δ_i^k, $\forall i \in I, k \in K \setminus \{N\}$ are binary variables defined to enforce the SOS2 condition through Constraints (27)-(30) that at most two adjacent λ_i^k, $\forall i \in I$ are positive and we have $\delta_i^k = 1$ if $G_i^{(k)} \le G_i \le G_i^{(k+1)}$, and $\delta_i^k = 0$ otherwise. Then the MTWC in the objective function of the model [EVFS-I] will be

$$MTWC^{\mathrm{I}} = C\left(\sum_{i \in I} \sum_{k=1}^{N} \lambda_i^k g(G_i^{(k)}) + \sum_{i \in I} \left((1-R_i)^b - (1-R_i+l_i)^b \right) + \sum_{i \in I} (1-Q_i)^b \right) \tag{32}$$

4.2. Outer-approximation method

The outer-approximation algorithm was initially proposed by Duran and Grossmann (1986) to find an ε-optimal solution to MINLP problems of a particular class. The main feature in the underlying mathematical structure of this particular class of problems (minimization problems) is the convexity of the nonlinear functions

involving continuous variables. For a general MINLP problem with convex terms both in the objective function and constraints, this algorithm obtains its ε-optimal solution by generating a sequence of non-increasing upper and non-decreasing lower bounds at multiple iterations until their difference does not exceed the pre-specified tolerance ε. Particularly, for the considered maximization problem [EVFS-I], since the concave terms appear only in the objective function, the outer-approximation algorithm can be applied more efficiently. Specifically, the model [EVFS-I] will be further transformed into a MILP model by approximating the concave terms in the objective function, i.e., $(1-R_i)^b-(1-R_i+l_i)^b$ and $(1-Q_i)^b$ in Eq. (32), with multiple linear functions. The ε-optimal solution can be readily obtained by solving the resultant MILP model using state-of-the-art MILP solvers like Gurobi.

To apply the outer-approximation method, we first define two auxiliary continuous variables A_i and B_i, $\forall i \in I$ as the proxy variables for $(1-R_i)^b-(1-R_i+l_i)^b$ and $(1-Q_i)^b$, respectively. The model [EVFS-I] can be rewritten by replacing $(1-R_i)^b-(1-R_i+l_i)^b$ and $(1-Q_i)^b$ in the objective function with A_i and B_i, and imposing Constraints (11)-(21), (25)-(31), and

$$A_i \le (1-R_i)^b-(1-R_i+l_i)^b, \quad \forall i \in I \tag{33}$$

$$B_i \le (1-Q_i)^b, \quad \forall i \in I \tag{34}$$

The MTWC in the objective function of the rewritten model can then be expressed by

$$MTWC^{\mathrm{II}} = C\left(\sum_{i\in I}\sum_{k=1}^{N}\lambda_i^k g(G_i^{(k)})+\sum_{i\in I}(A_i+B_i)\right) \tag{35}$$

For the sake of presentation, let $h(R_i)$ and $y(Q_i)$ denote the concave terms $(1-R_i)^b-(1-R_i+l_i)^b$ and $(1-Q_i)^b$, respectively, i.e., $h(R_i) := (1-R_i)^b-(1-R_i+l_i)^b$,

$\forall R_i \in [0, E], \forall i \in I$ and $y(Q_i) := (1-Q_i)^b, \forall Q_i \in [0, E], \forall i \in I$. Constraints (33) and (34) can thereby be relaxed by replacing the functions $h(R_i)$ and $y(Q_i)$ with many linear functions tangent to the concave curves $h(R_i)$ and $y(Q_i)$. Figure 8 illustrates the linearization of function $h(R_i)$ as an example. Those linear functions are grouped into two sets denoted by $\Omega = \{1, 2, ..., M-1, M\}$ and $V = \{1, 2, ..., P-1, P\}$ for $h(R_i)$ and $y(Q_i)$, respectively. Again, the generation of tangent points for tangent lines such that the approximation of the function $h(R_i)$ and $y(Q_i)$ can be controlled within a pre-specified tolerance $\hat{\varepsilon}$ is presented in Appendix B. Let $a_i^{(k)}$ and $b_i^{(k)}$ be the slope and intercept of the k^{th} tangent line of the curve $h(R_i)$ at the point $R_i^{(k)}$, i.e., $a_i^{(k)} = h'(R_i^{(k)})$ and $b_i^{(k)} = h(R_i^{(k)}) - h'(R_i^{(k)})R_i^{(k)}$. Thus Constraint (33) can be relaxed to be

$$A_i \le a_i^{(k)} R_i + b_i^{(k)}, \quad \forall i \in I, k \in \Omega \tag{36}$$

Similarly, Constraint (34) can be relaxed to be

$$B_i \le \bar{a}_i^{(k)} Q_i + \bar{b}_i^{(k)}, \quad \forall i \in I, k \in V \tag{37}$$

where $\bar{a}_i^{(k)}$ and $\bar{b}_i^{(k)}$ are the slope and intercept of the k^{th} tangent line of the curve $y(Q_i)$ at the point $Q_i^{(k)}$, i.e., $\bar{a}_i^{(k)} = y'(Q_i^{(k)})$ and $\bar{b}_i^{(k)} = y(Q_i^{(k)}) - y'(Q_i^{(k)})Q_i^{(k)}$.

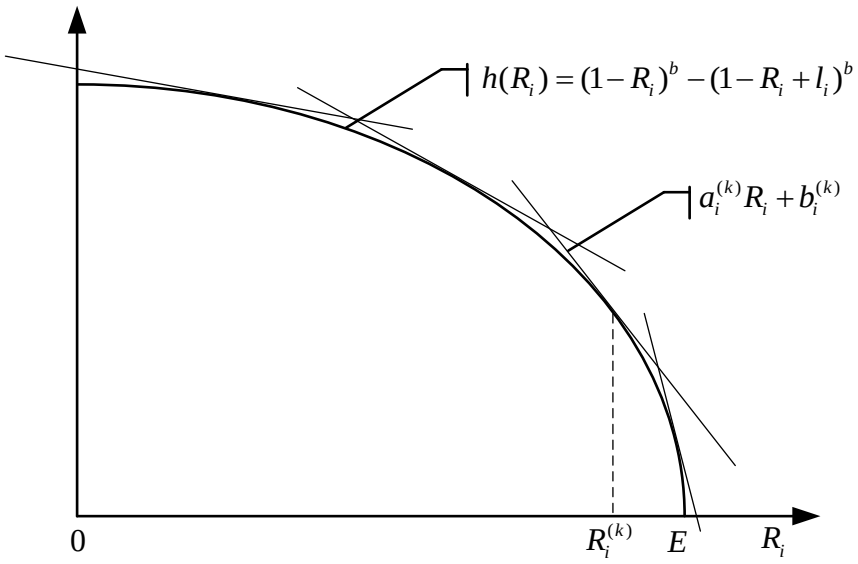

Figure 8. Illustration of the outer-approximation method

It can be seen that the original MINLP model [EVFS] has been transformed into the following MILP model by the piecewise linear approximation and outer-approximation methods, which can be efficiently solved by state-of-the-art MILP solvers like Gurobi:

[EVFS-II]

$$\max_{\mathbf{x,z,f,R,Q,e,\lambda,\delta,A,B}} PROFIT^{\mathrm{II}}(\mathbf{x,z,f,R,Q,e,\lambda,\delta,A,B}) = \sum_{i\in I} TP_i \times z_i - \sum_{i\in I} PC_i \times (1-z_i)$$
$$- \sum_{(i,j)\in A^r} RC_{ij} \times x_{ij} - FC \times f + C\left(\sum_{i\in I}\sum_{k=1}^{N} \lambda_i^k g(G_i^{(k)}) + \sum_{i\in I}(A_i + B_i) \right) \tag{38}$$

subject to Constraints (11)-(21), (25)-(31), and (36)-(37).

4.3. ε-optimal solution

This subsection demonstrates that we can obtain an ε-optimal solution to the MINLP model [EVFS] by solving the resultant MILP model [EVFS-II]. In the first place, we have the following proposition.

Proposition 1: Let $(\hat{\mathbf{x}},\hat{\mathbf{z}},\hat{\mathbf{f}},\hat{\mathbf{R}},\hat{\mathbf{Q}},\hat{\mathbf{e}},\hat{\boldsymbol{\lambda}},\hat{\boldsymbol{\delta}},\hat{\mathbf{A}},\hat{\mathbf{B}})$ denote an optimal solution to the MILP

model [EVFS-II] and $PROFIT^*$ denote the optimal objective value of the MINLP model [EVFS]. Then we have

$$PROFIT(\hat{\mathbf{x}},\hat{\mathbf{z}},\hat{\mathbf{f}},\hat{\mathbf{R}},\hat{\mathbf{Q}},\hat{\mathbf{e}}) \le PROFIT^* \le PROFIT^{\mathrm{II}}(\hat{\mathbf{x}},\hat{\mathbf{z}},\hat{\mathbf{f}},\hat{\mathbf{R}},\hat{\mathbf{Q}},\hat{\mathbf{e}},\hat{\boldsymbol{\lambda}},\hat{\boldsymbol{\delta}},\hat{\mathbf{A}},\hat{\mathbf{B}}) \quad (39)$$

Proof. Firstly, since the nonlinear terms are only in the objective function of the model [EVFS], we know that $(\hat{\mathbf{x}},\hat{\mathbf{z}},\hat{\mathbf{f}},\hat{\mathbf{R}},\hat{\mathbf{Q}},\hat{\mathbf{e}})$ will always be a feasible solution to the model [EVFS]. Therefore, we have

$$PROFIT(\hat{\mathbf{x}},\hat{\mathbf{z}},\hat{\mathbf{f}},\hat{\mathbf{R}},\hat{\mathbf{Q}},\hat{\mathbf{e}}) \le PROFIT^* \quad (40)$$

In addition, after adopting the piecewise linear approximation approach and the outer-approximation method, model [EVFS-II] can be interpreted as a relaxation of model [EVFS] defined as overestimating the objective function. Hence, its optimal objective value provides an upper bound on that of the model [EVFS]. Then we have

$$PROFIT^* \le PROFIT^{\mathrm{II}}(\hat{\mathbf{x}},\hat{\mathbf{z}},\hat{\mathbf{f}},\hat{\mathbf{R}},\hat{\mathbf{Q}},\hat{\mathbf{e}},\hat{\boldsymbol{\lambda}},\hat{\boldsymbol{\delta}},\hat{\mathbf{A}},\hat{\mathbf{B}}) \quad (41)$$

This completes the proof. □

Let $\hat{g}(G_i)=\sum_{k=1}^{N}\lambda_i^k g(G_i^{(k)})$, $\hat{h}(R_i)=\min_{k\in\Omega}\left\{a_i^{(k)}R_i+b_i^{(k)}\right\}$, and $\hat{y}(Q_i)=\min_{k\in V}\left\{\bar{a}_i^{(k)}Q_i+\bar{b}_i^{(k)}\right\}$ denote the corresponding piecewise linear approximation function for $g(G_i)$, $h(R_i)$, and $y(Q_i)$, respectively. The approximation error of the optimal solution can be controlled within a pre-specified tolerance $\varepsilon>0$, i.e.,

$$PROFIT^{\mathrm{II}}(\hat{\mathbf{x}},\hat{\mathbf{z}},\hat{\mathbf{f}},\hat{\mathbf{R}},\hat{\mathbf{Q}},\hat{\mathbf{e}},\hat{\boldsymbol{\lambda}},\hat{\boldsymbol{\delta}},\hat{\mathbf{A}},\hat{\mathbf{B}}) - PROFIT(\hat{\mathbf{x}},\hat{\mathbf{z}},\hat{\mathbf{f}},\hat{\mathbf{R}},\hat{\mathbf{Q}},\hat{\mathbf{e}}) \le \varepsilon \quad (42)$$

by properly selecting the breakpoints and tangent points for the piecewise linear segment and tangent line generation, respectively, such that $\hat{g}(G_i)-g(G_i)\le\hat{\varepsilon}$,

$\hat{h}(R_i) - h(R_i) \le \hat{\varepsilon}$, and $\hat{y}(Q_i) - y(Q_i) \le \hat{\varepsilon}$, where $\hat{\varepsilon} \le \frac{\varepsilon}{3 \times |I|}$.

Eq. (42) together with Eq. (39) jointly suggest that we can obtain the ε-optimal solution to the model [EVFS] by the proposed approaches, as summarized in the following proposition:

Proposition 2: For any exogenously specified tolerance ε>0, the proposed methods can obtain the ε-optimal solution to the model [EVFS], i.e.,

$$PROFIT(\hat{\mathbf{x}}, \hat{\mathbf{z}}, \hat{\mathbf{f}}, \hat{\mathbf{R}}, \hat{\mathbf{Q}}, \hat{\mathbf{e}}) \le PROFIT^* \le PROFIT(\hat{\mathbf{x}}, \hat{\mathbf{z}}, \hat{\mathbf{f}}, \hat{\mathbf{R}}, \hat{\mathbf{Q}}, \hat{\mathbf{e}}) + \varepsilon \qquad (43)$$

if we generate the linear segments and tangent lines subject to an error bound $\hat{\varepsilon} \le \frac{\varepsilon}{3 \times |I|}$.

As aforementioned, the algorithms to determine the breakpoints and tangent points for the linear segment and tangent line generation subject to a pre-specified error bound $\hat{\varepsilon}$, respectively, are presented in Appendix B for the readers' reference.

5. Numerical Experiments

This section presents the numerical experiments to evaluate the performance of the proposed model and solution method. The algorithm is coded in C++, calling Gurobi 9.0.0 on a personal computer with Intel (R) Core (TM) Duo 3.0 GHz CPU. The EVCARD in China and parameters setup is first introduced in Subsection 5.1. After that, the computational performance of the proposed solution method is assessed in Subsection 5.2. The necessity of incorporating the battery degradation into the fleet size determination of CSSs will be demonstrated in Subsection 5.3 in comparison with the model without considering battery degradation. Finally, sensitivity analysis of several key parameters on the system performance is examined in Subsection 5.4.

5.1. EVCARD in China and parameters setup

EVCARD, a popular one-way carsharing company in China, takes EV time-sharing rental as its core business. EVCARD operates more than 13,000 stations in about 65 cities with 50,000 new energy vehicles put into use at present, and the monthly order volume reaches 1.84 million. EVs can be rented by minute or day with different charge standards. In this study, the stations in three districts of Suzhou, namely, Kunshan, Xiangcheng, and Wujiang, are considered. The deployments of stations in these three districts are shown in Figure 9, with 70 stations in Kunshan, 27 stations in Xiangcheng, and 29 stations in Wujiang. Multiple stations are combined into one if the shortest path distances between them are within five-minute driving mileage, as we assume that there would be no rentals between these stations. This is implemented by Google Maps (Google, 2020) using the mode of 'driving' without considering traffic. After merging processing, 57 stations are obtained.

(a) Kunshan (b) Xiangcheng (c) Wujiang

Figure 9. Stations deployment in three districts of Suzhou

Let $\{1,2,...,57\}$ be the set of considered stations, from which we randomly generate the origin and destination stations of each rental $i \in I$, i.e., s_i^o and s_i^d. We assume the operating period is from 6 am to 10 pm, considering that most of the users have vehicle rental needs during this period. Particularly, if 6 am is taken as the time

benchmark and the time duration is measured in minutes, the departure time of each rental $i \in I$, i.e., t_i^o, is randomly generated from the integer set $\{0,1,...,960\}$ and the arrival time t_i^d is chosen as a uniformly random integer from the set $\{t_i^o + \Delta T_{min}, t_i^o + \Delta T_{min} + 1, ..., t_i^o + \Delta T_{max}\}$, where ΔT_{min} and ΔT_{max} are the minimum and maximum rental duration, respectively. If the destination station of the rental i is different from its origin station, we set ΔT_{min} to be the shortest travel time from the origin station to the destination station, which is obtained by Google Maps (Google, 2020). Otherwise ΔT_{min} is set to be 15 min to ensure the minimum profit from the perspective of a carsharing operator. All EVs are assumed to be equipped with a 16-kWh lithium-ion battery. The minimum SOC allowed for an EV, i.e., E_{min}, is assumed to be 0. With a fully charged battery, we assume that an EV can be driven for 150 min, with an average speed of 35 km per hour. ΔT_{max} is thus set to be 150 min, as we assume that the CSS is charged by rental duration and users would avoid leaving the EVs unused as much as possible during the rental period. A depleted battery is assumed to be fully charged in 150 min by a regular charging outlet. The charging and discharging rate of the battery expressed in percentage are both assumed to be a constant, i.e., $\frac{1}{150}/\min$, thus the charging amount and the electricity consumption are proportional to the charging and the trip (i.e., rental and relocation) duration respectively. The parameters related to battery wear cost in Eq. (3), i.e., a=694, b=0.795, μ=0.95, are adopted from Han et al. (2014). The price of battery is assumed to be 20,000¥.

Without loss of generality, we further assume that the service charge is 0.5¥/min according to the website of EVCARD (https://www.evcard.com/). The penalty for rejecting a rental is assumed to be 0.25¥/min, which is half of the revenue generated from the rental. The relocation cost and the daily fixed cost of an EV are set to be

0.3¥/min and 20¥/vehicle, respectively.

5.2. Computational performance of the proposed solution method

In this section, we compare the proposed approach, i.e., solving the resultant MILP model [EVFS-II] with the prevailing MILP solver Gurobi after applying the piecewise linear approximation approach and outer-approximation method, with the MINLP approach, which solves the model [EVFS] directly by using Knitro, an especially versatile nonlinear solver offering a range of state-of-the-art algorithms and options for working with smooth objective and constraint functions in continuous and integer variables. Problems of different sizes indicated by the number of rentals (#TotalRent) are used to test the performance of the proposed solution method and MINLP approach. For a particular-size problem, ten instances are randomly generated and the average results are reported. Moreover, different values of $\hat{\varepsilon}$ are adopted for the proposed approach to analyze its effects on the quality of solutions. The preliminary numerical experiments indicated that both the MINLP approach and the proposed approach could obtain the optimal solution in a few seconds under a relatively small demand (e.g., 10). Nevertheless, when the demand increases beyond a certain value (e.g., 25), the MINLP approach can no longer produce the optimal solution. In more detail, it obtains a feasible solution by the built-in heuristic algorithms in a few minutes, and after the feasible solution is produced, it will not improve the solution quality even within the time limit of 12 hours. Regarding the proposed approach, for the problems with the number of rentals larger than a specific value (e.g., 50), no improvement in the solution quality could be made after 1 hour of running time because the solution values obtained within 1 hour and 12 hours are almost the same, and the difference between the solution values achieved within 15 minutes and 1 hour is not significant. Hence, we set the time limit to be 15 minutes to compare the solution values obtained by the two approaches. Specifically, two performance measures, i.e., the objective value and the computation

time (in seconds), are compared. Let Obj_Knitro and Obj_Gurobi be the objective value obtained by the MINLP approach and the proposed approach, respectively. For a more intuitive comparison, the ratio of Obj_Gurobi to Obj_Knitro, i.e., Obj_Gurobi/Obj_Knitro, is also reported. This value must be equal to 1 if both approaches can find an optimal solution within 15 min. A value larger than 1 indicates that the solution obtained by the proposed approach is better than that achieved by the MINLP approach, and vice versa.

The results are tabulated in Table 2. Overall, it shows that the proposed approach obtains much better solutions within 15 min compared with the MINLP approach except for the smallest-size instances with 10 rentals. This outcome demonstrates the superiority of the proposed approach. For the smallest-size problem, both approaches can obtain the optimal solution within the time limit, with the proposed approach taking much less time at the values of $\hat{\varepsilon}$ larger than 0.001. It is interesting that the computation time for the proposed approach dramatically decreases from hundreds of seconds to a fraction of a second when the value of $\hat{\varepsilon}$ increases to above 0.001. This can be explained by the fact that a smaller tolerance $\hat{\varepsilon}$ indicates more binary variables for the piecewise linear approximation approach in Subsection 4.1, which may dominate the computational efficiency for the small-size problems. For the larger-size problems, within the time limit of 15 min, the MINLP approach can no longer obtain the optimal solution. The proposed approach, however, can still find the optimal solution to the instances with 25 rentals at all values of $\hat{\varepsilon}$ except 0.001. For a specific-size problem, it can be observed that the objective value produced by the proposed approach is not sensitive to the tolerance $\hat{\varepsilon}$ when the value of it is not smaller than 0.25. However, this is not true for the values of $\hat{\varepsilon}$ not greater than 0.25 within which the highest objective value, indicating the best solution, can generally be obtained at the value of $\hat{\varepsilon}$=0.01, although there exist exceptions for the smallest-size instances with 10 rentals. Hence, $\hat{\varepsilon}$=0.01 will be employed to carry out the following analysis.

Regarding the quality of solutions, the objective value achieved by the proposed approach is at least 1.43 times that of the MINLP approach without considering the problem with 10 rentals. Therefore, the proposed approach shows a visible advantage over the MINLP approach on the whole in solving the tactical problem proposed by this study.

Table 2. Comparison of computational performance between the MINLP approach and the proposed approach

#TotalRent	MINLP approach		Our approach			
	Obj_ Knitro	Comp_ Time	$\hat{\varepsilon}$	Obj_ Gurobi	Comp_ Time	Obj_Gurobi/ Obj_Knitro
10	309.45	1.22	0.001	309.98	128.89	1.00
			0.01	309.89	0.17	1.00
			0.1	309.29	0.03	1.00
			0.25	306.43	0.03	0.99
			0.5	306.43	0.03	0.99
25	545.48	900.08	0.001	795.09	900.02	1.46
			0.01	795.70	60.88	1.46
			0.1	792.91	6.74	1.45
			0.25	782.06	6.45	1.43
			0.5	782.06	6.42	1.43
50	984.43	900.15	0.001	1602.68	900.03	1.63
			0.01	1608.85	900.03	1.63
			0.1	1608.36	900.02	1.63
			0.25	1578.93	900.03	1.60
			0.5	1578.93	900.02	1.60
75	1524.83	900.21	0.001	2377.52	900.04	1.56
			0.01	2386.84	900.04	1.57
			0.1	2376.69	900.03	1.56
			0.25	2330.86	900.04	1.53
			0.5	2330.86	900.04	1.53
100	2060.40	900.11	0.001	3199.48	900.58	1.55
			0.01	3222.99	900.04	1.56
			0.1	3188.14	900.04	1.55
			0.25	3118.40	900.05	1.51
			0.5	3118.40	900.04	1.51
125	2547.99	900.14	0.001	3985.09	900.08	1.56
			0.01	3993.38	900.06	1.57
			0.1	3975.84	900.13	1.56
			0.25	3865.23	900.08	1.52
			0.5	3865.23	900.10	1.52

5.3. Impact of battery degradation consideration

In this section, we first numerically explore how the incorporation of battery wear cost influences the tactical decision of fleet size, i.e., the main concern of this study, and justify the benefit of battery degradation consideration to the profitability of CSSs. Then we investigate how the parameters in the battery wear function, i.e., the battery price and battery cycle efficiency, affect the influence of battery degradation consideration on the profitability and fleet size of CSSs. We formulate a model that is similar to the model [EVFS], but without taking the battery wear cost into account, referred to as [EVFS$^{w/o}$] thereafter. For ease of comparison, we rename the model considering the battery degradation, i.e., [EVFS], as [EVFS^{w}] in this subsection. In addition, the parameter setting in this section is the same as that specified in Subsection 5.1, and ten instances are randomly generated for a particular number of rentals (#TotalRent) and the average results are reported.

5.3.1. Impact on the fleet size determination

To investigate the impact of battery degradation consideration on the fleet size decision of CSSs, we solve the model [EVFS^{w}] and the model [EVFS$^{w/o}$] respectively by randomly generating the same instances and compare the fleet size obtained from the two models. For the sake of presentation, let 'FleetSize^{w}' and 'FleetSize$^{w/o}$' be the fleet size obtained by solving the model [EVFS^{w}] and the model [EVFS$^{w/o}$], respectively. The ratio of FleetSize^{w} to FleetSize$^{w/o}$, i.e., FleetSize_Ratio, is adopted to evaluate the impact of the battery degradation consideration on the fleet size determination of CSSs.

Table 3 presents the impact of battery degradation consideration on the tactical decision of fleet size. It can be seen from Table 3 that all the ratios, i.e., FleetSize^{w}/FleetSize$^{w/o}$, are larger than 1.7, which implies that the consideration of battery degradation will result in the substantial expansion of fleet size. This suggests, when the battery degradation is further taken into account, the carsharing operator

should adopt a larger fleet size to serve rentals in order to avoid the extensive charging and discharging processes and realize the ultimate profit maximization. These findings demonstrate the necessity of incorporating the battery degradation into the fleet size determination of CSSs and hence validate the significance of this study.

Table 3. Impact of battery degradation consideration on the fleet size determination

#TotalRent	$FleetSize^{w}$	$FleetSize^{w/o}$	FleetSize_Ratio
10	7.4	4.6	1.75
25	17.0	9.7	1.83
50	31.1	17.0	1.94
75	44.9	23.1	1.85
100	57.1	30.8	1.86
125	69.2	37.3	1.75

5.3.2. Impact on the profitability improvement

In order to measure the profitability improvement simply brought by the battery degradation consideration during the operation period, we compare the profits obtained from the model [$EVFS^{w}$] and the model [$EVFS^{w/o}$] given the same fleet size. That's to say, under a certain demand, the number of EVs is set to be the same constant in the two models and the fleet investment is considered as a sunk cost. After solving the two models by randomly generating the same instances, we calculate the battery wear cost for the model [$EVFS^{w/o}$] and subtract the battery wear cost from the objective function value. Finally, the daily profits of the carsharing operator based on the two models can be obtained, both with the battery wear cost included. Again, let '$Profit^{w}$' and '$Profit^{w/o}$' denote the daily profit of the carsharing operator obtained from the model [$EVFS^{w}$] and the model [$EVFS^{w/o}$], respectively. The gap of profits indicated by 'Profit_Gap' is defined as '$(Profit^{w} - Profit^{w/o})/Profit^{w}$'. It can be used to assess the benefit of the battery degradation consideration to the profitability of CSSs. Specifically, the fleet size is set to be 7, 16, 28, 40, 55, 70 under the demand of 10, 25, 50, 75, 100, 125, respectively.

The profitability improvement brought by the battery degradation consideration is

shown in Table 4. We can conclude from Table 4 that the consideration of battery degradation does enhance the profitability of CSSs because all the gaps of profits are larger than 7%. The largest gap in profit can be as high as 13.97% when the number of rentals is 50. It appears that the gap of profits generally shows an upward trend along with the rising of demand except for the scenario with 50 rentals. This may indicate that the profitability of CSSs can be improved more significantly by considering battery degradation when the demand is higher. This result further verifies the value of this study. However, we caution that the influence of battery degradation consideration on the profitability and fleet size of CSSs may largely depend on the parameters in the battery wear cost function. The values of these parameters should be carefully chosen based on empirical studies in the future. In Subsection 5.3.3, we will continue to test how the parameters in the battery wear cost function affect the impact of battery degradation consideration.

Table 4. Impact of battery degradation consideration on the profitability of CSSs

#TotalRent	$Profit^{w}$ (¥/day)	$Profit^{w/o}$ (¥/day)	Profit_Gap (%)
10	438.40	405.61	7.48
25	1095.14	1002.80	8.43
50	2141.90	1842.65	13.97
75	3198.89	2870.35	10.27
100	4339.47	3827.43	11.80
125	5484.27	4813.94	12.22

To further affirm the circumvention of the extensive charging and discharging processes brought by the consideration of battery degradation given a certain fleet size, three performance metrics, i.e., the total rental duration (TotalRentalTime), the total charging duration (TotalChargeTime), and the total relocation duration (TotalRelocationTime), are compared between the two models under the demand of 125. The results are illustrated in Figure 10. It shows that the total rental durations of the fleet obtained from the two models are almost the same. The total charging duration under the model [$EVFS^{w}$], however, shows a sharp decrease compared to the model

[EVFS$^{w/o}$]. This is because when the battery wear cost is taken into account in the objective function, unnecessary charging processes will be circumvented for the sake of profit maximization. Regarding the total relocation duration, the result of the model [EVFS^{w}] is slightly higher than the model [EVFS$^{w/o}$]. These findings indicate that a comparable number of rentals are served in the two models and the battery degradation consideration results in the reduced charging processes, which contributes to the profitability improvement of CSSs.

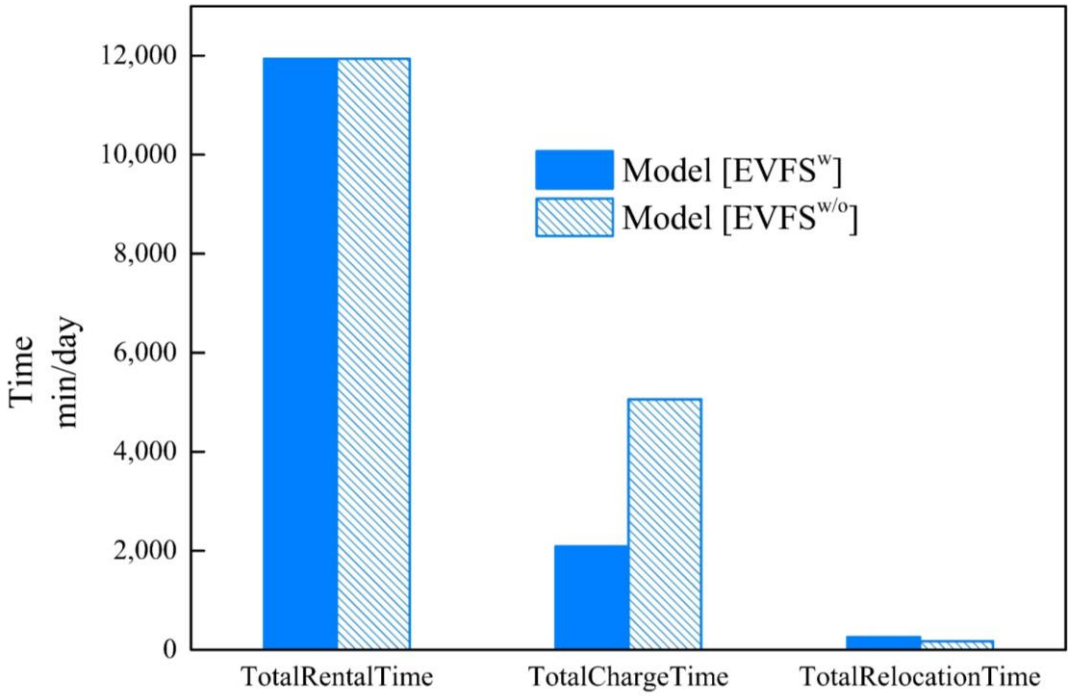

Figure 10. Comparison between the model [EVFS^{w}] and the model [EVFS$^{w/o}$] under the demand of 125

5.3.3. Impact of parameters in the battery wear cost function

This subsection will investigate how the parameters in the battery wear cost function, i.e., the battery price and battery cycle efficiency, affect the impact of battery degradation consideration on the fleet size determination and profitability of CSSs. Due to the inter-dependency relationship between the battery price and the fixed cost of EVs, different battery prices should be associated with different EV fixed costs. More

specifically, under the demand of 125, three values of battery price and daily fixed cost of EV, i.e., 12,000 & 12, 16,000 & 16, 20,000 & 20, and three values of battery cycle efficiency, i.e., 0.91, 0.93, 0.95, are adopted to test their effects on the influence of battery degradation consideration on the fleet size determination and profitability of CSSs.

Table 5 shows how the two parameters influence the impact of battery degradation consideration on fleet size determination. We can see that with the increase of battery price & daily fixed cost of EV, the ratio of fleet size grows gradually, indicating that the battery degradation consideration has a greater effect on the fleet size determination under a higher value of battery price & daily fixed cost of EV. In addition, when the battery cycle efficiency decreases from 0.95 to 0.91, the ratio rises steadily. These results suggest that the impact of battery degradation on the fleet size determination of CSSs is largely influenced by battery price & daily fixed cost of EV and battery cycle efficiency.

Compared with the fleet size, the parameters in the battery wear cost function influence less the impact of battery degradation consideration on the profitability of CSSs. As shown in Table 6 where $Profit^{w}$ and $Profit^{w/o}$ are obtained by solving the model [$EVFS^{w}$] and the model [$EVFS^{w/o}$] under the fleet size of 70, respectively, the impact of battery degradation consideration on the profitability of CSSs is affected by the two parameters in the battery wear cost function. It can be seen that the gap of profits increases along with the growth of battery price & daily fixed cost of EV, while it almost remains stable when the battery cycle efficiency varies. This implies that the profitability improvement brought by the battery degradation consideration is more significant when the battery price & daily fixed cost of EV is higher, and it appears not sensitive to the battery cycle efficiency.

Table 5. Impact on the influence of battery degradation consideration on the fleet size determination

Price&EVCost (¥&¥/vehicle/day)	Efficiency	FleetSize^{w}	FleetSize$^{w/o}$	FleetSize_Ratio
12,000&12	0.95	73.6	42.7	1.72
16,000&16	0.95	70.7	38.9	1.82
20,000&20	0.95	69.2	37.3	1.86
20,000&20	0.93	70.9	37.3	1.90
20,000&20	0.91	74.0	37.3	1.98

Table 6. Impact on the influence of battery degradation consideration on the profitability

Price&EVCost (¥&¥/vehicle/day)	Efficiency	Profit^{w} (¥/day)	Profit$^{w/o}$ (¥/day)	Profit_Gap
12,000&12	0.95	5659.60	5254.26	0.07
16,000&16	0.95	5570.97	5034.10	0.10
20,000&20	0.95	5482.78	4813.94	0.12
20,000&20	0.93	5461.82	4766.08	0.13
20,000&20	0.91	5442.88	4715.03	0.13

5.4. Sensitivity analysis

In this section, we will investigate how the key parameters, i.e., the daily fixed cost of EV & battery price, battery cycle efficiency, service charge, and relocation cost, affect the performance of one-way electric CSSs. Several performance indicators, which include the daily profit of carsharing operator, the number of satisfied rentals (#SatisRent), the satisfied ratio (#SatisRent/#TotalRent), the optimal EV fleet size (FleetSize), the usage rate of EV (#SatisRent/FleetSize), the daily battery wear cost per vehicle (WearCost), the daily rental duration per vehicle (RentalTime), the daily relocation duration per vehicle (RelocationTime) as well as the daily charging duration per vehicle (ChargeTime), are reported for ease of comparison and evaluation. Unless stated otherwise, the parameter setting is the same with Subsection 5.1 except that we randomly generate 10 instances with 125 rentals.

Effect of the daily fixed cost of EV & battery price

Since the high capital investment in EV fleet poses a major problem for many carsharing operators and the wear cost of the battery is closely related to the price of it,

we first explore the effect of the daily fixed cost of EV & battery price on the performance of one-way electric CSSs. The results are tabulated in Table 7. It can be seen that the increase of daily fixed cost of EV & battery price leads to the significantly decreased profit of CSSs, indicating the dominating impact of the daily fixed cost of EV & battery price on the profitability of CSSs. It is worth noting that the satisfied ratio is first stable at 1 and then decreases to 0.998 when the daily fixed cost of EV & battery price increases from 10&10,000 to 28&28,000, with the 26&26,000 being the turning point. This suggests that under the current parameter setting, all rentals would be served for the sake of profit maximization, even if the daily fixed cost of EV & battery price rises to 26&26,000. With the growth of the daily fixed cost of EV and battery price, the fleet size reduces with fluctuation while the rental, relocation, and charging duration generally increase significantly, eventually resulting in the overall upward trend of the usage rate and the significant increase of battery wear cost. We caution that the rising battery wear cost results from the dual effects of the growing daily fixed cost of EV & battery price and the time-related indicators. This demonstrates that the climbing daily fixed cost of EV & battery price may prompt the carsharing operators to acquire a smaller fleet size and serve rentals by more frequent relocation and charging operations.

Table 7. Effect of daily fixed cost of EV and battery price on the performance of one-way electric CSSs

EVCost&Price (¥/vehicle/day&¥)	Profit (¥/day)	#SatisRent	#SatisRent/#TotalRent	FleetSize	#SatisRent/FleetSize	WearCost (¥/vehicle/day)	RentalTime (min/vehicle/day)	RelocationTime (min/vehicle/day)	ChargeTime (min/vehicle/day)
10&10,000	5007.70	125.0	1.000	75.7	1.65	2.02	157.78	2.21	20.64
12&12,000	4807.04	125.0	1.000	73.6	1.70	2.85	162.32	3.07	24.48
14&14,000	4612.37	125.0	1.000	72.8	1.72	3.59	164.06	3.44	26.38
16&16,000	4407.60	125.0	1.000	70.7	1.77	4.81	169.05	4.25	31.09
18&18,000	4217.98	125.0	1.000	71.2	1.76	5.24	167.70	4.46	30.18
20&20,000	4003.10	125.0	1.000	69.2	1.81	6.88	172.68	5.13	35.69
22&22,000	3819.76	125.0	1.000	69.6	1.80	7.33	171.68	5.22	34.50
24&24,000	3639.43	125.0	1.000	69.9	1.79	7.85	171.15	5.13	33.99
26&26,000	3422.73	125.0	1.000	68.8	1.82	9.24	173.75	6.06	37.00
28&28,000	3212.94	124.8	0.998	67.0	1.87	11.26	178.40	6.29	41.62

Effect of battery cycle efficiency

As an important indicator of battery cycle life, cycle efficiency influences the battery wear cost greatly, as shown by Eq. (3). We thus investigate the variations of the performance indicators with respect to the growth of battery cycle efficiency, and the results are presented in Table 8. It illustrates that when the battery cycle efficiency rises, the profit shows a growing trend in general with the number of satisfied rentals remaining at 125. This indicates that under the current parameter setting, serving all rentals will be most conducive to profit maximization, even if the battery cycle efficiency is reduced to 0.9. The fleet size, however, decreases with minor fluctuations, leading to an overall upward trend of EV usage rate. All the time-related indicators averagely increase in a modest manner, and the battery wear cost grows gradually, in a fluctuating way, if any. This appears contrary to the fact that the increase of battery cycle efficiency should result in the declining battery wear cost, as indicated by Eq. (3). Kindly note that in addition to the battery cycle efficiency, charging and discharging processes corresponding to the time-related indicators are another two factors affecting the battery wear cost. A larger cycle efficiency means a lower battery wear cost under the same operating condition, which may allow longer charging and discharging (i.e., rental and relocation) duration per vehicle by smaller fleet size in pursuit of profit maximization. As a result, the battery wear cost shows an increasing trend under the combined effects of rising battery cycle efficiency and time-related indicators. It can be found that installing batteries with higher cycle efficiency in EVs has a similar positive effect on the profitability of CSSs to acquiring EVs with lower daily fixed cost & battery price to a certain degree. However, the variation magnitude of the profit is less than that resulted from the variation of the daily fixed cost of EV & battery price. The daily fixed cost of EV & battery price and the battery cycle efficiency should be considered comprehensively by the carsharing operators to increase the profitability.

Table 8. Effect of battery cycle efficiency on the performance of one-way electric CSSs

Efficiency	Profit (¥/day)	#SatisRent	#SatisRent/#TotalRent	FleetSize	#SatisRent/FleetSize	WearCost (¥/vehicle/day)	RentalTime (min/vehicle/day)	RelocationTime (min/vehicle/day)	ChargeTime (min/vehicle/day)
0.9	3990.44	125.0	1.000	74.1	1.69	5.41	161.20	4.31	25.24
0.91	3997.67	125.0	1.000	74.0	1.69	5.33	161.42	4.42	25.40
0.92	4007.41	125.0	1.000	73.5	1.70	5.54	162.87	4.48	26.66
0.93	4006.71	125.0	1.000	70.9	1.77	6.30	168.56	4.69	31.34
0.94	4008.01	125.0	1.000	70.5	1.77	6.36	169.72	5.06	32.47
0.95	4003.10	125.0	1.000	69.2	1.81	6.88	172.68	5.13	35.69
0.96	4017.75	125.0	1.000	68.3	1.84	7.02	175.19	5.34	37.17
0.97	4022.11	125.0	1.000	68.6	1.83	6.89	174.71	5.33	37.25
0.98	4039.08	125.0	1.000	67.4	1.86	7.05	177.14	5.22	38.88
0.99	4036.05	125.0	1.000	66.4	1.89	7.43	180.05	5.70	41.89

Effects of service charge and relocation cost

In addition to the daily fixed cost of EV and battery price and the battery cycle efficiency, we also test how the variations of the service charge and relocation cost influence the performance of electric CSSs. The results are presented in Table 9 and Table 10. In Table 9, we can see that the carsharing companies would be in the red if the service charge is set to be below 0.18¥/min. With the increase of service charge, the satisfied ratio rises slowly until to 1 and profit grows dramatically, while the variations of time-related indicators, fleet size, EV usage rate, and battery wear cost are somehow arbitrary. This indicates that the determination of fleet size, the main concern in our study, may be less affected by the charge standard under the current parameter setting. Compared with the service charge, the impacts of the relocation cost on the performance of electric CSSs are more significant. The variations of the above performance indicators with respect to the relocation cost are summarized in Table 10. It shows that all the performance indicators remain almost stable at a particular value when the relocation cost is not smaller than 1.5¥/min. Particularly, the relocation time is zero under this scenario, implying that if the relocation cost is high enough, no relocation operation would be implemented to pursue profit maximization. When the relocation cost increases from 0.1¥/min to 1.3¥/min, the profit appears to vary arbitrarily, with fewer rentals satisfied in general. This seems unreasonable as a higher relocation cost would result in a lower profit. Kindly note that the proposed method can only obtain the ε-optimal solution to the problem in question and the obtained profits may not be the global optimal values. Along with the increase of relocation cost within the value of 0.15¥/min, the trade-off effect between fleet size and vehicle relocation is distinct because their variation trends are opposite, i.e., when the relocation cost grows, the fleet size increases significantly while the relocation duration shows an obvious decrease. The carsharing operators are thus suggested to serve rentals by acquiring more EVs, i.e., less vehicle relocation, for the sake of profit maximization under a high relocation

cost. Accordingly, larger fleet size and less vehicle relocation lead to the lower usage rate of EVs, the reduced rental and charging duration, as well as the falling battery wear cost.

Table 9. Effect of service charge on the performance of one-way electric CSSs

Charge (¥/min)	Profit (¥/day)	#SatisRent	#SatisRent/#TotalRent	FleetSize	#SatisRent/FleetSize	WearCost (¥/vehicle/day)	RentalTime (min/vehicle/day)	RelocationTime (min/vehicle/day)	ChargeTime (min/vehicle/day)
0.1	-758.06	124.5	0.996	71.7	1.74	5.81	166.45	4.62	30.28
0.18	208.23	124.7	0.998	71.7	1.74	5.78	166.55	4.25	30.08
0.26	1145.37	124.9	0.999	70.4	1.78	6.40	169.92	4.95	33.32
0.34	2092.76	124.9	0.999	68.8	1.82	7.05	173.82	5.22	36.74
0.42	3056.31	125.0	1.000	69.5	1.80	6.67	172.12	5.19	34.57
0.5	4003.10	125.0	1.000	69.2	1.81	6.88	172.68	5.13	35.69
0.58	4970.81	125.0	1.000	69.7	1.80	6.58	171.44	4.85	34.04
0.66	5922.25	125.0	1.000	69.1	1.81	6.76	172.99	5.23	35.17
0.74	6874.74	125.0	1.000	68.9	1.82	6.91	173.44	5.08	35.74
0.82	7836.39	125.0	1.000	70.2	1.78	6.39	170.33	4.79	33.09

Table 10. Effect of relocation cost on the performance of one-way electric CSSs

RelocationCost (¥/min)	Profit (¥/day)	#SatisRent	#SatisRent/#TotalRent	FleetSize	#SatisRent/FleetSize	WearCost (¥/vehicle/day)	RentalTime (min/vehicle/day)	RelocationTime (min/vehicle/day)	ChargeTime (min/vehicle/day)
0.1	4025.51	125.0	1.000	67.8	1.86	8.12	177.28	7.72	42.16
0.3	4003.10	125.0	1.000	69.2	1.81	6.88	172.68	5.13	35.69
0.5	4042.01	124.9	0.999	73.2	1.71	4.85	163.18	2.92	24.86
0.7	4053.35	125.0	1.000	76.6	1.63	3.74	155.91	1.80	19.04
0.9	4042.04	124.7	0.998	79.3	1.57	3.03	150.53	1.35	15.45
1.1	4029.73	124.6	0.997	80.9	1.54	2.92	147.54	0.89	14.80
1.3	4018.45	124.5	0.996	84.0	1.48	2.73	142.13	0.30	13.88
1.5	4018.92	124.5	0.996	85.8	1.45	2.64	139.18	0.00	13.41
1.7	4018.30	124.5	0.996	86.0	1.45	2.59	138.84	0.00	13.17
1.9	4018.36	124.5	0.996	85.8	1.45	2.65	139.16	0.00	13.42

6. Conclusions

This study investigated the EVFS problem for the one-way electric CSSs by taking battery degradation into account. Instead of charging the EVs as extensively as possible, we first proposed the 'on-demand' charging strategy, which allows EVs to be charged as needed to reduce the battery wear cost incurred from battery degradation. An MINLP model with both concave and convex terms in the objective function was then developed to maximize the profit of carsharing operators by simultaneously determining the fleet size, vehicle relocation operations, and charging strategies of EVs. The consideration of nonlinear battery wear cost made the proposed model not easily solvable to optimality by commercial solvers. We thus linearized the considered model by applying the piecewise linear approximation approach and the outer-approximation method on the convex and concave terms, respectively. The resultant MILP model can finally be solved by state-of-the-art solvers like Gurobi. At last, numerical experiments based on the carsharing company EVCARD in China were conducted. In more detail, the computational performance of the proposed model and solution method was first demonstrated. Then we made a comparison between the proposed model and the one without taking the battery degradation into account. The comparison results indicate that the consideration of battery degradation will increase the profitability of the CSSs and expand the fleet size significantly. This finding demonstrates the necessity of incorporating the battery degradation into the fleet size determination of CSSs and hence validates the significance of this study. Finally, the effects of the daily fixed cost of EV & battery price, battery cycle efficiency, service charge, and relocation cost on the performance of electric CSSs were analyzed. The results reveal that the increase of daily fixed cost of EV & battery price may prompt the carsharing operators to acquire a smaller fleet size and serve rentals by more frequent relocation and charging operations; Installing batteries with higher cycle efficiency in EVs would lead to a decrease of fleet size and the growth of time-related indicators as well as daily battery

wear cost per vehicle; Under a higher relocation cost, the carsharing operators should acquire more EVs to serve rentals and thus conduct less vehicle relocation for the sake of profit maximization, while the service charge under the current parameter setting has less effect on the fleet size.

Further research work can be undertaken in several aspects. First, efficient algorithms or heuristic methods remain to be developed for implementation in large-scale problems in the future. Second, in the current study, EVs are assigned to users for the sake of profit maximization without considering the choice behavior of users. While in reality, users may have their own preference for a particular EV for their trips. Incorporating the choice behavior of users would make the study more align with reality. Finally, it would be practically significant to consider the uncertainty of user demand and operating parameters in future research work, e.g., rental, relocation, and charging duration, electricity consumption, etc.

Acknowledgements

This research is supported by the National Natural Science Foundation of China (No. 71901189), the Research Grants Council of the Hong Kong Special Administrative Region, China (PolyU 25207319), and the Hong Kong Polytechnic University (UAHJ).

Appendix A: Notation

I	Set of rentals
A^r	Set of relocation operations connecting any two rentals that are compatible both in terms of travel time and electricity consumption
A^0	Set of dummy links connecting the dummy node and all the rentals
i, j	Indices for rental
(i, j)	Index for link
n_0	Index for the dummy node
FC	The fixed daily amortized cost of an EV
s_i^o	Pick-up station of rental i
s_i^d	Drop-off station of rental i
t_i^o	Departure time of rental i

t_i^d	Arrival time of rental i
l_i	Electricity consumption of rental i
TP_i	Net profit of rental i
PC_i	Incurred penalty for rejecting rental i
l_{ij}	Electricity consumption of relocation operation from the drop-off station of rental i to the pick-up station of rental j
t_{ij}	Relocation time from the drop-off station of rental i to the pick-up station of rental j
RC_{ij}	Relocation cost from the drop-off station of rental i to the pick-up station of rental j
CR	Charging rate
DR	Discharging rate
M_1, M_2	Big numbers
E	The usable battery capacity
E_{min}	The minimum SOC allowed for an EV
E_{comf}	The minimum SOC value above which users are free from range anxiety
WC	Battery wear cost incurred during charging or discharging process
WC_r	Battery wear cost of an EV over the entire operation period
TWC	The total battery wear cost of all EVs over the entire operation period
$W(l)$	Battery wear density function with respect to the SOC l that represents the battery wear cost per unit energy transfer at the SOC l
l_{init}	The initial SOC of battery before the charging or discharging process
l_{ulti}	The ultimate SOC of battery after the charging or discharging process
BP	Battery price
BS	Battery size
μ	Battery cycle efficiency
a, b	Battery-dependent parameters that are acquired experimentally
$\varepsilon, \hat{\varepsilon}$	Pre-specified tolerances
$g(G_i)$	Denote the convex term $-(1-G_i)^b$, i.e., $g(G_i) := -(1-G_i)^b$, $\forall G_i \in [0, E],\ \forall i \in I$
$h(R_i)$	Denote the concave term $(1-R_i)^b - (1-R_i+l_i)^b$, i.e., $h(R_i) := (1-R_i)^b - (1-R_i+l_i)^b,\ \forall R_i \in [0, E],\ \forall i \in I$
$y(Q_i)$	Denote the concave term $(1-Q_i)^b$, i.e., $y(Q_i) := (1-Q_i)^b$, $\forall Q_i \in [0, E],\ \forall i \in I$
$\hat{g}(G_i)$	Piecewise linear approximation function for the curve $g(G_i)$
$\hat{h}(R_i)$	Piecewise linear approximation function for the curve $h(R_i)$
$\hat{y}(Q_i)$	Piecewise linear approximation function for the curve $y(Q_i)$

$a_i^{(k)}$	The slope of the k^{th} tangent line of the curve $h(R_i)$
$b_i^{(k)}$	The intercept of the k^{th} tangent line of the curve $h(R_i)$
$\bar{a}_i^{(k)}$	The slope of the k^{th} tangent line of the curve $y(Q_i)$
$\bar{b}_i^{(k)}$	The intercept of the k^{th} tangent line of the curve $y(Q_i)$
K	Set of breakpoints for the linear segments of the curve $g(G_i)$
Ω	Set of tangent lines of the curve $h(R_i)$
V	Set of tangent lines of the curve $y(Q_i)$
k	Index for breakpoint of the curve $g(G_i)$ or tangent line of the curves $h(R_i)$ and $y(Q_i)$
N	Number of breakpoints for the linear segments of the curve $g(G_i)$
M	Number of tangent lines of the curve $h(R_i)$
P	Number of tangent lines of the curve $y(Q_i)$
f	Integer decision variable representing fleet size of EVs
z_i	Binary decision variable that equals 1 if rental i is satisfied, and 0 otherwise
x_{ij}	Binary decision variable that equals 1 if an EV is relocated from the drop-off station of rental i to the pick-up station of rental j, and 0 otherwise
R_i	Continuous decision variable denoting SOC of an EV rightly before serving the rental i
Q_i	Continuous decision variable denoting SOC of an EV rightly before the relocation operation originated from the drop-off station of rental i
e_i^o	Continuous decision variable denoting amount of electricity charged at the pick-up station of rental i
e_i^d	Continuous decision variable denoting amount of electricity charged at the drop-off station of rental i
G_i	Continuous variable denoting the SOC of an EV rightly after arriving at the origin station of rental i
λ_i^k, δ_i^k	Binary variables for the application of piecewise linear approximation approach
A_i	Proxy variable for the concave term $(1-R_i)^b-(1-R_i+l_i)^b$ in the objective function (24)
B_i	Proxy variable for the concave term $(1-Q_i)^b$ in the objective function (24)
ΔT_{min}	The minimum rental duration
ΔT_{max}	The maximum rental duration

Appendix B: Algorithms for model linearization

The determination of the breakpoints for linear segments of the convex terms in the objective function (10) is shown in **Algorithm 1**. *FindSegmentPoint* is a recursive function to find the set of breakpoints for the linear segments of the convex curve $g(G_i)$. In each recursion step, this function will return a unique point in the domain $G_i \in [G_i^{(L)}, G_i^{(U)}]$ with the maximum error for approximating the convex function $g(G_i)$ using the linear segment specified by the two endpoints of the interval, if the maximum error is larger than $\hat{\varepsilon}$. The sub-function *SegmentLine* will return the slope and intercept of the line across points $(G_i^{(L)}, g(G_i^{(L)}))$ and $(G_i^{(U)}, g(G_i^{(U)}))$. *SlopeEquivalentPoint* returns the point with the maximum error for approximating the convex function $g(G_i)$ using the linear segment specified by the above two endpoints. *ApproximationValue* calculates the approximate value for the function $g(G_i)$ at this unique point.

Algorithm 1: Pseudocode for finding the set of breakpoints $\boldsymbol{P}$ for linear segment generation.

Initialize $\boldsymbol{P} \leftarrow \{G_i^{(L)}, G_i^{(U)}\}$;
Function $[\boldsymbol{P}] = FindSegmentPoint(G_i^{(L)}, G_i^{(U)}, \boldsymbol{P})$
  $[s, c] = SegmentLine(G_i^{(L)}, G_i^{(U)})$;
  $G_i = SlopeEquivalentPoint(g(G_i), s)$;
  $\hat{g}(G_i) = ApproximationValue(s, c, G_i)$;
  $Error = \hat{g}(G_i) - g(G_i)$;
  If $Error > \hat{\varepsilon}$, then \\ If the maximal error is larger than the threshold, add the corresponding point to set $\boldsymbol{P}$, and execute the above procedure for two subintervals $[G_i^{(L)}, G_i]$, $[G_i, G_i^{(U)}]$
    $\boldsymbol{P} \leftarrow G_i$;
    $[\boldsymbol{P}] = FindSegmentPoint(G_i^{(L)}, G_i, \boldsymbol{P})$

10 $[\boldsymbol{P}] = FindSegmentPoint(G_i, G_i^{(U)}, \boldsymbol{P})$

11 End if

12 End function

Analogously, the procedure for determining the tangent points for tangent lines of the concave terms in the objective function (10) is presented in **Algorithm 2**, taking the function $h(R_i)$ as an example. *FindTangentPoint* is a recursive function to determine the set of tangent points in the domain $R_i \in [R_i^{(L)}, R_i^{(U)}]$ for the tangent lines of the concave curve $h(R_i)$. Due to the infinite slope of the curve $h(R_i)$ at the point $R_i = E$, *FindTangentPoint* first returns a new $R_i^{(U)}$ that ensures the approximation error at the point $R_i = E$ is no larger than $\hat{\varepsilon}$, which is determined by the sub-function $FindNewR_i^{(U)}$. The function *TangentLine* returns the slope and intercept of the tangent lines at points $(R_i^{(L)}, h(R_i^{(L)}))$ and $(R_i^{(U)}, h(R_i^{(U)}))$. *Intersection* calculates the coordinate value of the intersection of the above two tangent lines. The function *FindTangentPoint* will return the point corresponding to the intersection, i.e., the point at which the error for approximating the concave function $h(R_i)$ using the outer-approximation envelope formulated by the above two tangent lines is maximal when $R_i^{(L)} \le R_i \le R_i^{(U)}$, if the approximation error at the point is larger than $\hat{\varepsilon}$.

Algorithm 2: Pseudocode for finding the set of tangent points $\boldsymbol{T}$ for tangent line generation.

1 Initial $\boldsymbol{T} \leftarrow \{R_i^{(L)}, R_i^{(U)}\}$;

2 Function $[\boldsymbol{T}] = FindTangentPoint(R_i^{(L)}, R_i^{(U)}, \boldsymbol{T})$

3 If $R_i^{(U)} = E$, then \\ Since the slope of curve $h(R_i)$ at point E is infinite, we need to find a new $R_i^{(U)}$ if $R_i^{(U)}=E$ to ensure the approximation error at point E is no larger than $\hat{\varepsilon}$.

4 $[R_i^0] = FindNewR_i^{(U)}(h(R_i), E, \hat{\varepsilon})$;

5 End if

6 $R_i^{(U)} \leftarrow R_i^0$

7 $[s_1, c_1] = TangentLine(R_i^{(L)})$;

8 $[s_2, c_2] = TangentLine(R_i^{(U)})$;

9 $[R_i, \hat{h}(R_i)] = Intersection(s_1, c_1, s_2, c_2)$;

10 $Error = \hat{h}(R_i) - h(R_i)$;

11 If $Error > \hat{\varepsilon}$, then \\ If the error is larger than the threshold value, add the corresponding point R_i to set $\boldsymbol{P}$, and execute the above procedure for the two subintervals $[R_i^{(L)}, R_i]$ and $[R_i, R_i^{(U)}]$.

12 $\boldsymbol{T} \leftarrow R_i$;

13 $[\boldsymbol{T}] = FindTangentPoint(R_i^{(L)}, R_i, \boldsymbol{T})$

14 $[\boldsymbol{T}] = FindTangentPoint(R_i, R_i^{(U)}, \boldsymbol{T})$

15 End if

16 End function

References

AutoBleue, 2020. https://www.auto-bleue.org/en (accessed 08.05.2020).

Barré, A., Deguilhem, B., Grolleau, S., Gérard, M., Suard, F., Riu, D., 2013. A review on lithium-ion battery ageing mechanisms and estimations for automotive applications. *Journal of Power Sources* 241, 680-689.

BlueSG, 2020. https://www.bluesg.com.sg (accessed 08.05.2020).

Boyacı, B., Zografos, K.G., 2019. Investigating the effect of temporal and spatial flexibility on the performance of one-way electric carsharing systems. *Transportation Research Part B: Methodological* 129, 244-272.

Boyacı, B., Zografos, K.G., Geroliminis, N., 2015. An optimization framework for the development of efficient one-way car-sharing systems. *European Journal of Operational Research* 240(3), 718-733.

Boyacı, B., Zografos, K.G., Geroliminis, N., 2017. An integrated optimization-simulation framework for vehicle and personnel relocations of electric carsharing systems with reservations. *Transportation Research Part B: Methodological* 95,

214-237.

Bruglieri, M., Colorni, A., Luè, A., 2014. The relocation problem for the one-way electric vehicle sharing. *Networks* 64(4), 292-305.

Bruglieri, M., Pezzella, F., Pisacane, O., 2017. Heuristic algorithms for the operator-based relocation problem in one-way electric carsharing systems. *Discrete Optimization* 23, 56-80.

Bruglieri, M., Pezzella, F., Pisacane, O., 2019. An adaptive large neighborhood search for relocating vehicles in electric carsharing services. *Discrete Applied Mathematics* 253, 185-200.

Car2Go, 2020. https://www.car2go.com/US/en (accessed 08.05.2020).

Cass, D., Grudnoff, M., 2017. If you build it, they will charge. https://www.tai.org.au/sites/default/files/P233%20If%20you%20build%20it%20they%20will%20charge%20FINAL%20-%20October%202017.pdf (accessed 08.05.2020).

Dill, J., McNeil, N., Howland, S., 2019. Effects of peer-to-peer carsharing on vehicle owners' travel behavior. *Transportation Research Part C: Emerging Technologies* 101, 70-78.

Duran, M.A., Grossmann, I.E., 1986. An outer-approximation algorithm for a class of mixed-integer nonlinear programs. *Mathematical Programming* 36(3), 307-339.

EVCARD, 2020. https://www.evcard.com (accessed 08.05.2020).

Gambella, C., Malaguti, E., Masini, F., Vigo, D., 2018. Optimizing relocation operations in electric car-sharing. *Omega* 81, 234-245.

GoFun, 2020. https://www.shouqiev.com (accessed 08.05.2020).

Google, 2020. Google Maps. https://www.google.com.hk/maps (accessed 08.05.2020).

Guéret, C., Prins, C., Sevaux, M., 2000. Applications of optimization with Xpress-MP. http://citeseerx.ist.psu.edu/viewdoc/download?doi=10.1.1.69.9634&rep=rep1&type=pdf (accessed 15.09.2020).

Han, S., Han, S., Aki, H., 2014. A practical battery wear model for electric vehicle charging applications. *Applied Energy* 113, 1100-1108.

Hua, Y., Zhao, D., Wang, X., Li, X., 2019. Joint infrastructure planning and fleet management for one-way electric car sharing under time-varying uncertain demand. *Transportation Research Part B: Methodological* 128, 185-206.

Huang, K., An, K., de Almeida Correia, G.H., 2020. Planning Station Capacity and Fleet Size of One-way Electric Carsharing Systems with Continuous State of Charge Functions. *European Journal of Operational Research* 287(3), 1075-1091.

Jorge, D., Correia, G., Barnhart, C., 2012. Testing the validity of the MIP approach for locating carsharing stations in one-way systems. *Procedia - Social and Behavioral Sciences* 54, 138-148.

Jorge, D., Correia, G.H., Barnhart, C., 2014. Comparing optimal relocation operations with simulated relocation policies in one-way carsharing systems. *IEEE Transactions on Intelligent Transportation Systems* 15(4), 1667-1675.

Laporte, G., Meunier, F., Calvo, R.W., 2018. Shared mobility systems: an updated survey. *Annals of Operations Research* 271(1), 105-126.

Li, X., Ma, J., Cui, J., Ghiasi, A., Zhou, F., 2016. Design framework of large-scale one-way electric vehicle sharing systems: A continuum approximation model. *Transportation Research Part B: Methodological* 88, 21-45.

Lu, R., Correia, G.H.d.A., Zhao, X., Liang, X., Lv, Y., 2020. Performance of one-way

carsharing systems under combined strategy of pricing and relocations. *Transportmetrica B: Transport Dynamics*, 1-19.

Montoya, A., Guéret, C., Mendoza, J.E., Villegas, J.G., 2016. A multi-space sampling heuristic for the green vehicle routing problem. *Transportation Research Part C: Emerging Technologies* 70, 113-128.

Mounce, R., Nelson, J.D., Practice, 2019. On the potential for one-way electric vehicle car-sharing in future mobility systems. *Transportation Research Part A: Policy* 120, 17-30.

Mourad, A., Puchinger, J., Chu, C., 2019. A survey of models and algorithms for optimizing shared mobility. *Transportation Research Part B: Methodological* 123, 323-346.

Nourinejad, M., Zhu, S., Bahrami, S., Roorda, M.J., 2015. Vehicle relocation and staff rebalancing in one-way carsharing systems. *Transportation Research Part E: Logistics and Transportation Review* 81, 98-113.

Pelletier, S., Jabali, O., Laporte, G., Veneroni, M., 2017. Battery degradation and behaviour for electric vehicles: Review and numerical analyses of several models. *Transportation Research Part B: Methodological* 103, 158-187.

Repoux, M., Kaspi, M., Boyacı, B., Geroliminis, N., 2019. Dynamic prediction-based relocation policies in one-way station-based carsharing systems with complete journey reservations. *Transportation Research Part B: Methodological* 130, 82-104.

Schiffer, M., Walther, G., 2017. The electric location routing problem with time windows and partial recharging. *European Journal of Operational Research* 260(3), 995-1013.

Smove, 2020. https://www.smove.sg (accessed 08.05.2020).

Wang, L., Liu, Q., Ma, W., 2019. Optimization of dynamic relocation operations for one-way electric carsharing systems. *Transportation Research Part C: Emerging Technologies* 101, 55-69.

Wang, L., Zhong, H., Ma, W., Zhong, Y., Wang, L., 2020. Multi-source data-driven prediction for the dynamic pickup demand of one-way carsharing systems. *Transportmetrica B: Transport Dynamics* 8(1), 90-107.

Xu, M., Meng, Q., 2019. Fleet sizing for one-way electric carsharing services considering dynamic vehicle relocation and nonlinear charging profile. *Transportation Research Part B: Methodological* 128, 23-49.

Xu, M., Meng, Q., Liu, Z., 2018. Electric vehicle fleet size and trip pricing for one-way carsharing services considering vehicle relocation and personnel assignment. *Transportation Research Part B: Methodological* 111, 60-82.

Xu, M., Yang, H., Wang, S., 2020. Mitigate the range anxiety: Siting battery charging stations for electric vehicle drivers. *Transportation Research Part C: Emerging Technologies* 114, 164-188.

Yang, S., Wu, J., Sun, H., Qu, Y., Li, T., 2021. Double-balanced relocation optimization of one-way car-sharing system with real-time requests. *Transportation Research Part C: Emerging Technologies* 125, 103071.

Zhang, D., Liu, Y., He, S., 2019. Vehicle assignment and relays for one-way electric car-sharing systems. *Transportation Research Part B: Methodological* 120, 125-146.

Zhao, M., Li, X., Yin, J., Cui, J., Yang, L., An, S., 2018. An integrated framework for electric vehicle rebalancing and staff relocation in one-way carsharing systems:

Model formulation and Lagrangian relaxation-based solution approach. *Transportation Research Part B: Methodological* 117, 542-572.